Palaeogeography, Palaeoclimatology, Palaeoecology 566 (2021) 110209

Contents lists available at ScienceDirect

Palaeogeography, Palaeoclimatology, Palaeoecology

journal homepage: www.elsevier.com/locate/palaeo

Variable redox conditions as an evolutionary driver? A multi-basin comparison of redox in the middle and later Cambrian oceans (Drumian-Paibian)

Matthew A. LeRoy [a], Benjamin C. Gill [a,*], Erik A. Sperling [b], N. Ryan McKenzie [c], Tae-Yoon S. Park [d]

[a] Department of Geosciences, Virginia Polytechnic Institute and State University, Blacksburg, VA 24061, USA
[b] Department of Geological Sciences, Stanford University, Stanford, CA 94305, USA
[c] Department of Earth Sciences, University of Hong Kong, Pokfulham, Hong Kong, China
[d] Division of Polar Earth-System Sciences, Korea Polar Research Institute, 26 Songdomirae-ro Yeonsu-gu, Incheon 21990, Republic of Korea

ARTICLE INFO

Keywords:
Cambrian
Marine redox
Sedimentary redox
Iron speciation
DICE
SPICE

ABSTRACT

The middle to later Cambrian (Drumian-Jiangshanian Ages, 505–490 Ma) was a time of unique evolutionary dynamics that remain enigmatic. This interval records unusually high rates of faunal turnover that produced a "plateau" within the broader trajectory of rapidly increasing biodiversity seen across the Cambrian Explosion and Great Ordovician Biodiversification Event (GOBE). The oceans during this time are generally thought to have been less oxygenated than later in the Phanerozoic, yet knowledge of oceanic redox structure and the influence this exerted upon the biosphere remains limited. Importantly, this interval also encompasses two large carbon cycle perturbations—the DICE and SPICE events— that are thought to involve the expansion of anoxic and, more specifically euxinic regions in the ocean. Despite this supposition, direct characterization of redox conditions across this time remains limited. Here we explore these conditions using new and previously published Fe-speciation data from seven basins distributed across five paleocontinents representing a range of depositional conditions. Our analysis reveals anoxia was a common and persistent feature of deeper-water environments and that it was generally absent from shallower-waters across this timespan. An exception to this broad pattern is seen during the SPICE when these deeper-water anoxic conditions expanded into shallower-water environments. These anoxic conditions were dominantly ferruginous and rare instances of euxinia were spatiotemporally limited to environments of high productivity, low clastic sedimentation and high sulfate availability within a generally low-sulfate ocean. Intriguingly, during these events faunal turnover was concentrated in inner-shelf areas suggesting a mechanistic link to the variable redox conditions characteristic of these environments. More broadly this instability in nearshore environments appears a likely cause of the high rates of faunal turnover seen across the later Cambrian and into the Early Ordovician, but further detailed paleontological and redox investigation of these environments are needed to adequately evaluate this view.

1. Introduction

1.1. Background

The oxygenation state of Earth's ocean–atmosphere system is widely regarded as an important first-order control upon the development and evolutionary trajectory of the biosphere from the earliest prokaryotes through the much later advent of complex metazoans. While the broad outlines of this trajectory have come into increasingly sharper focus in recent years, important details within this understanding remain uncertain. There is a long-standing hypothesis that oxygen levels increased significantly during two major pulses prior to the Phanerozoic Eon (542 Ma-present). The first pulse is thought to have occurred at ~2.4 Ga during the Great Oxidation Event (Holland, 2002) and the second occurred sometime after the latter half of the Neoproterozoic (after 800 Ma) (e.g. Lenton et al., 2014). Outstanding questions concerning the

* Corresponding author.
E-mail addresses: mleroy@vt.edu (M.A. LeRoy), bcgill@vt.edu (B.C. Gill), esper@stanford.edu (E.A. Sperling), ryan00@hku.hk (N.R. McKenzie), typark@kopri.re.kr (T.-Y.S. Park).

https://doi.org/10.1016/j.palaeo.2020.110209
Received 31 March 2020; Received in revised form 25 November 2020; Accepted 28 November 2020
Available online 4 January 2021

second rise in oxygenation are the precise timing of when oxygen rose in the atmosphere, when the deeper portions of the oceans were subsequently oxygenated, whether these were unidirectional or more dynamic with time, and whether these changes were sufficient or necessary to drive contemporaneous biological evolution (Cole et al., 2020). Evidence exists for at least transient deep ocean oxygenation in the latest Ediacaran (Canfield et al., 2007), but there is also evidence pointing to more persistent deep ocean oxygenation occurring much later in the Paleozoic, possibly as late as the Devonian, in conjunction with the rise of significant vascular land plants communities (Dahl et al., 2010; Krause et al., 2018; Sperling et al., 2015a). More recently it has been suggested that persistent oxygenation of the deeper oceans may have been decoupled from atmospheric oxygenation and delayed until much later (i.e., during the Mesozoic), despite earlier rises in atmospheric pO_2 (Lu et al., 2018). Uncertainty in the timeline of marine oxygenation is not trivial: the early Paleozoic interval in question represents a time of several major (and numerous smaller) evolutionary radiations and extinctions including: the Cambrian Explosion and the Great Ordovician Biodiversification Event (GOBE), as well as the end-Ordovician and Late Devonian mass extinctions, all of which may be in part tied to the oxygenation history of the oceans (see Fig. 1A for context).

A fundamental challenge that gives rise to much of this uncertainty regarding the past oxygenation state of the ocean–atmosphere system is the nature of the geologic data available to make such reconstructions, which rely largely upon indirect paleoredox proxies. The isotopic compositions of carbon ($\delta^{13}C$) and sulfur ($\delta^{34}S$) in marine sediments, in particular, are thought to faithfully record global seawater trends, and are used to inform modeling approaches (e.g., GEOCARBSULF, COPSE) that leverage our understanding of the relationships between the biogeochemical cycles of carbon, sulfur and oxygen over geologic timescales. However, these approaches can produce a range of model solutions depending upon how they are parameterized, as well as the quality and volume of data available to input (Fig. 1B). For instance, the basic GEOCARBSULF model calculates atmospheric oxygen concentrations in the early Paleozoic both considerably higher than modern (Schachat et al., 2018) and considerably lower than modern (Krause et al., 2018) based on different treatments of sulfur cycling. Due to this, our best efforts still are only able to bracket a range of potential pO_2 levels that remain consistent with the input data and other geochemical proxies (e.g., trace metal abundances and isotopic compositions in black shales). Most importantly, within these modeled ranges of atmospheric oxygen concentrations it is difficult to accurately predict the spatial distribution of marine oxygen availability (redox structure) and consequently how prone—or not—different areas of the ocean were to the development or persistence of anoxia. More detailed knowledge of this aspect of ancient ocean chemistry and its attendant consequences for the biosphere are needed to better understand important evolutionary dynamics during this time.

In an effort to shed light on some of these crucial nuances, the aim of this study is to characterize local redox conditions during a key early Paleozoic interval (middle to late Cambrian) that lies between the evolutionary radiations of the Cambrian Explosion and the Great Ordovician Biodiversification Event (GOBE) (Fig. 1A). This interval is also situated after the hypothesized Neoproterozoic rise in atmospheric oxygen, but before the rise that occurred during the Middle to Late Paleozoic (Fig. 1B). Moreover, while there has been an intensive focus on characterizing ocean redox during the latest Ediacaran and earliest Cambrian (Terreneuvian - Stage 4) (Chen et al., 2015; Cheng et al., 2016, 2017; Dahl et al., 2019; Feng et al., 2014; Hammarlund et al., 2017; He et al., 2019; Jin et al., 2016, 2017; Li et al., 2017; Och et al., 2013, 2016;

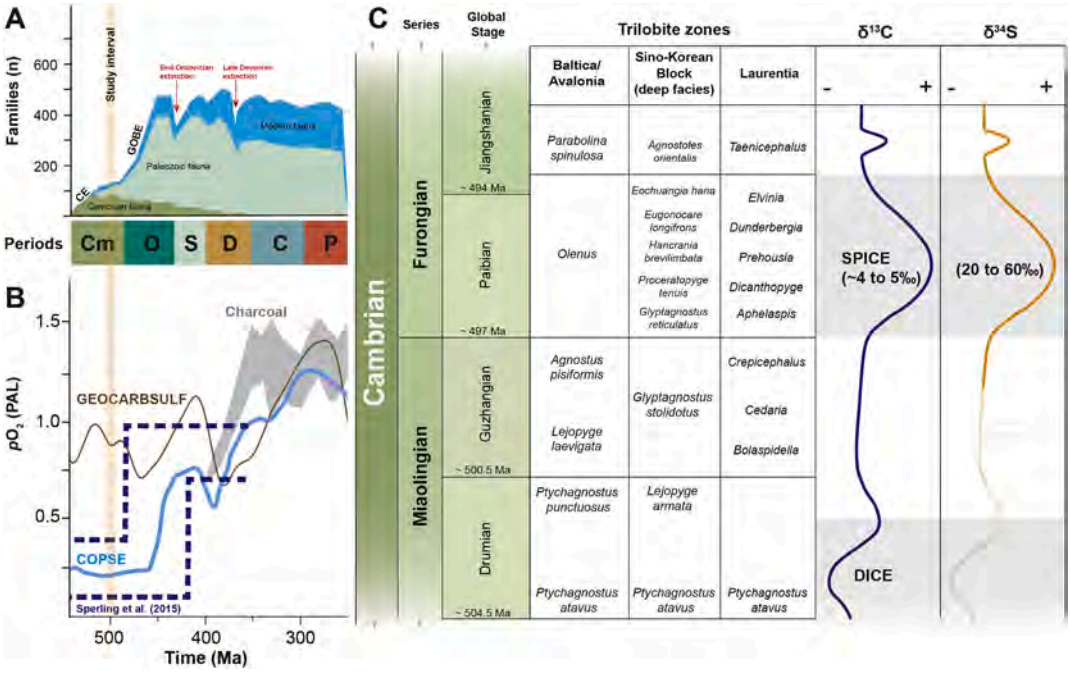

Fig. 1. Contextual details of the Cambrian time interval explored in this study. (A) The Sepkoski curve of overall familial diversity through the Paleozoic Era subdivided by marine evolutionary faunas: Cambrian (dark green), Paleozoic (light green) and Modern (blue). Modified from Servais et al. (2010) after Sheehan (1996). Note the temporal range of the study interval (orange shaded box in A & B) lies between the rapid diversifications of the Cambrian Explosion (CE) and the Great Ordovician Biodiversification Event (GOBE). These stages are depicted in detail in panel C. (B) Estimates of Paleozoic atmospheric oxygen concentration (pO_2) derived from modeling approaches and available proxy data modified from Lu et al. (2018). Estimates are shown relative to present atmospheric level (PAL; 20.9% O_2 by volume). GEOCARBSULF and COPSE model results are from Berner (2006) and Lenton et al. (2018), respectively. Charcoal proxy record from Glasspool and Scott (2010). (C) Generalized stage-level chrono-, bio-, and chemostratigraphic features of the investigated Cambrian interval of the four locations used in this study. Age estimates for stage boundaries are based on the 2019 International Commission on Stratigraphy International Chronostratigraphic Chart (v2019/05). See Section 2 of the main text for references and further information. (For interpretation of the references to colour in this figure legend, the reader is referred to the web version of this article.)

Sperling et al., 2018; Wang et al., 2012), there has been significantly less effort to ascertain marine redox conditions during the rest of the Cambrian. Those that have reconstructed the history of marine redox during latter half of the Cambrian have primarily focused on reconstructing and modeling the marine carbon and sulfur isotope records (Gill et al., 2007, 2011; Hough et al., 2006; Hurtgen et al., 2009; Li et al., 2018; Peng et al., 2016). The lack of more diverse redox proxy data from the later Cambrian limits our understanding of the redox structure of oceans and the potential links between it and changes in the biosphere during this time.

Studies of marine redox in the earlier Cambrian suggest a persistence of deep ocean anoxia despite evidence for oxygenation in the later Ediacaran, so a next logical question is how far into the early Paleozoic did these conditions persist? For this task we employ the iron speciation proxy to reconstruct local redox conditions within several geographically widespread sedimentary basins during the middle to later Cambrian (Wuliuan to Jiangshanian International Stages). Furthermore, these study locations encompass a range of different environmental parameters such as: paleobathymetry, sediment supply, organic carbon availability, and location relative to the nearest open ocean basin during this intriguing portion of the Cambrian.

1.2. Middle and Late Cambrian evolutionary events and the SPICE

This study specifically focuses on the middle to late Cambrian: Drumian through Lower Jiangshanian Stages. Understanding the oxygenation state of the ocean–atmosphere system during this interval is key for several reasons. First, it contains two large, globally-expressed carbon cycle perturbations—the DICE (Drumian Carbon Isotope Excursion) and SPICE (Steptoean Positive Carbon Isotope Excursion) events. Second, the interval is also a time of abnormally high rates of turnover in marine fauna (Bambach et al., 2004; Harper et al., 2019).

The DICE occurred during the lower Drumian Stage and is recorded as a negative excursion in the isotopic composition of sedimentary carbonate and organic carbon identified in sections worldwide (Ahlberg et al., 2009; Babcock et al., 2007; Faggetter et al., 2018; Howley and Jiang, 2010; Lehnert et al., 2013; Li et al., 2019; Pagès et al., 2016; Pagès and Schmid, 2016; Zhu et al., 2004). It also occurred during a transgressive event in Laurentia and Australia (Howley and Jiang, 2010; Pagès and Schmid, 2016). The DICE has been suggested to be caused by the oxidation of dissolved organic carbon during the shoaling of deep anoxic waters on the shelves (Li et al., 2019) or the transgression of deeper waters with ^{12}C-enriched dissolved inorganic carbon onto the shelf (Howley and Jiang, 2010), although neither model has been thoroughly evaluated. Biomarker and redox sensitive metal data suggest at least local development of euxinic conditions during the DICE in Australia (Pagès et al., 2016), but whether this change is more widespread is yet to be explored.

The SPICE spans the Paibian Stage and is recorded as large positive excursions in the isotopic composition of carbon- and sulfur-bearing sedimentary materials (δ^{13}C and δ^{34}S) in strata of this age worldwide (Fig. 1C; Ahlberg et al., 2009; Gill et al., 2011; Li et al., 2018; Ng et al., 2014; Peng et al., 2016; Pruss et al., 2019; Pulsipher et al., 2021; Saltzman et al., 2000; Woods et al., 2011; Wotte and Strauss, 2015). The records of these excursions exhibt regional differences in magnitude and absolute values that may reflect regional differences in ocean chemistry, uncomformities, and/or diagenetic alteration. (Gill et al., 2011; Schiffbauer et al., 2017; Pulsipher et al., 2021). The initiation of these isotope excursions appear to be temporally coupled with a significant extinction event recognized on several paleocontinents—the end-Marjuman extinction (Gerhardt and Gill, 2016; Gill et al., 2011; Saltzman et al., 1998; Saltzman et al., 2000; Zhu et al., 2004). These combined features are hypothesized to be associated with an expansion of the areal extent of seafloor anoxia (Dahl et al., 2014; Gill et al., 2011; LeRoy and Gill, 2019) and to a possible net rise in atmospheric oxygen related to organic carbon and pyrite burial across the event (Saltzman et al., 2011).

As previously mentioned, the second noteworthy feature of this time period is that it represents an evolutionary "plateau" between the rapid increases in biological diversity and complexity of the Cambrian Explosion that precedes it and the subsequent evolutionary radiation of the GOBE that followed (Bambach et al., 2004; Harper et al., 2019). This evolutionary pattern has been attributed to particularly high rates of extinction and diversification, which served to impede overall increases in standing biodiversity (Bambach et al., 2004). It should be noted that Harper et al. (2019) highlights the paucity of fossiliferous deposits and a lack of detailed taxonomic studies of Furongian strata as potential biases that contribute to the biodiversity patterns during this interval. However recent analysis of marine diversity during this interval that explicitly account for sampling intensity and fossil preservation supports the initial suggestion of low biodiversity accumulation during this interval (Rasmussen et al., 2019). These observations have led workers to propose that extreme and highly variable environmental conditions (e.g., recurring expansions of oceanic anoxia, high atmospheric pCO_2, surface oceans with lower calcite and aragonite saturation, and greenhouse climate) may have been a characteristic feature of this interval (Edwards et al., 2018; Gill et al., 2011; McKenzie et al., 2014; Pruss et al., 2010; Saltzman et al., 2015) and perhaps even an important long-term driver of evolutionary novelty and innovation through increased diversification following extinctions (Wood and Erwin, 2018).

In light of these considerations, this contribution aims to directly characterize redox conditions in different regions of the middle to later Cambrian ocean to better understand the relationship between environmental conditions and evolutionary change during this time. In order to reconstruct local water column redox conditions, we present new geochemical datasets, which include iron speciation, organic carbon isotopes and contents, and pyrite sulfur isotopes, from two middle to upper Cambrian sedimentary successions. These data are analyzed along with previously published geochemical datasets from five other coeval sedimentary successions deposited in basins with a wide geographic distribution. This comparison allows us to more broadly assess the distribution of different water column redox conditions in inner and outer shelf environments and basinal environments through the middle to later Cambrian. We then go on to use this data compilation to explore the potential relationships between this redox structure and its variation through time to the carbon cycle perturbations and biological events during the middle to later Cambrian. Notably, our study differs from the previous studies of this time interval because they focus primarily on interpreting redox during specific intervals in the middle to later Cambrian (specifically the DICE and SPICE). Our study also relies on a large compilation of iron speciation data (a proxy for local water column redox conditions), while other studies rely on reconstructing global scale changes in redox based on the marine carbon, sulfur, and uranium isotope records (Dahl et al., 2014; Gill et al., 2007, 2011; Hough et al., 2006; Hurtgen et al., 2009; Li et al., 2018; Peng et al., 2016).

2. Geologic context

2.1. Study locations

For this study we examine geochemical data from seven middle through upper Cambrian sedimentary succession from the paleocontinents of Avalonia, Baltica, Laurentia, and Gondwana. During this time Avalonia, Baltica, and southern Laurentia were situated along the margins of the Iapetus Ocean in the Southern Hemisphere, while northern Laurentia and northern Gondwana (the Sino-Korean Block and Australia) were located close to the paleoequator within the larger Panthalassic Ocean (Fig. 2, Cocks and Torsvik (2016). Here we present new data from the Stockingford Shale Group (Drumian-Jiangshanian) of central England (Nuneaton, U.K) representing east Avalonia and from the Machari Formation (Drumian-Jiangshanian) of South Korea from the Sino-Korean Block. We compare these data to previously published data from the Drumian-Jiangshanian portions of the Alum Shale (Scania,

Fig. 2. Paleogeographic reconstruction of the Late Cambrian Earth modified from Cocks and Torsvik (2016). The localities with new data presented in this study are indicated by black stars: Avalonia (abbreviated AV; central England) and Sino-Korean Block (abbreviated SKB; Sino-Korean Block). Localities included in the compilation with previously published data are indicated by white stars: Baltica (southern Sweden, Gill et al., 2011); Southern Laurentia (Ohio and Kentucky, USA, LeRoy and Gill, 2019); Northern Laurentia (Utah, U.S.A.; Sperling et al. 2015b) and Yukon, Canada; SGP database]; and Northern Gondwana (abbreviated AUS; Northern Territory, Australia; Creveling et al. (2014)).

Sweden) of Baltica (Gill et al., 2011); the Drumian Wheeler Shale (Utah, U.S.A) of northern Laurentia (Sperling et al., 2015b); the Drumian Arthur Creek Formation (Northern Territory, Australia) of northern Gondwana (Creveling et al., 2014); the Guzhangian-Paibian Nolichucky and Eau Claire Formations (Ohio and Kentucky, U.S.A) of southern Laurentia (LeRoy and Gill, 2019). Iron speciation data from Guzhangian-Jiangshanian Road River Group (Yukon, Canada) of northern Laurentia (Strauss et al., 2020) were obtained from the database of the Sedimentary Geochemistry and Paleoenvironments Project; SGP). In the remainder of this section, we give additional context for the successions with new data that we present here. For additional details on the geological context of the units where data have been previously reported, we refer the reader to those publications.

2.2. Outwoods Shale, Mancetter Grits and Abbey Shales of Avalonia

The Stockingford Shale Group, which includes the Outwoods Shale, Mancetter Grits and Abbey Shales, consists primarily of alternating intervals of organic-rich, sulfidic (dark gray) and organic-lean, sulfide-poor (light gray) siliciclastic mudrocks occasionally interrupted by cm-scale sand- and siltstone beds. Taylor and Rushton (1971) attributed the pattern of alternating light and dark mudstones to fluctuating redox conditions at the seafloor and its effect on bioturbation and the preservation of reduced sedimentary components (e.g., organic carbon and pyrite). The sediments comprising the Stockingford Shale Group were deposited in the distal portions of a stable but gently subsiding shelf located at a high paleolatitude (~60°S, Fig. 2; Cocks and Torsvik, 2016). The biostratigraphy of Rushton (1978, 1983) and Rushton et al., (1999) established that deposition of this unit was broadly continuous from the middle through later Cambrian producing a nearly 300 m thick stratigraphic sequence. Further details about this unit can be found in Woods et al. (2011) and references within.

2.3. Machari Formation of South Korea

The Machari Formation is a mixed carbonate-siliciclastic sequence comprised of argillaceous lime mudstones/dolostones, laminated gray and black shales, and thin beds of bioclastic grainstone. This unit is part of the Yeongwol Group and represents deposition that occurred in the distal portions (greatest distance from paleoshore) of the Taebaeksan Basin, an intracratonic basin in which sediments accumulated during the Cambrian-Ordovician (Chough et al., 2000). The generally more basinal facies of Yeongwol Group are thought to be correlative to shallower water facies found in the Taebaek Group, currently further to the east (Chough et al., 2000). The Machari Formation itself was deposited from the middle through late Cambrian (Wuliuan through Jiangshanian International Stages) (Hong, 2014; Hong and Choi, 2015). Despite the considerable time interval represented by this formation (~15 Myrs) it is highly condensed with a total stratigraphic thickness that is only around 10 m at the Deoksang locality we investigated for this study—an indication that sediment fluxes to this location were extremely low (Hong, 2014; Hong and Choi, 2015). See Choi et al. (2016) and Chough et al. (2000) and references therein for further details about this formation and interpretation of its depositional environment.

3. Methods

3.1. Materials, sampling and previous work

In this contribution we present two new geochemical studies of middle through upper Cambrian stratigraphic intervals in the Stockingford Shale Group of England and the Machari Formation of South Korea. Importantly, a detailed biostratigraphic framework is available for each of these units and locations in the form of trilobite biostratigraphy (Rushton, 1978, 1983 for the Stockingford Shale Group, and Hong, 2014 and Hong and Choi, 2015 for the Machari Formation). For further comparison and analysis, we also incorporate into our discussion (Section 5) data compiled from the five additional successions noted above that record deposition during this time interval. Previous work has established the carbon isotope chemostratigraphy of these units and identified the SPICE within the Alum Shale (Ahlberg et al., 2009), Stockingford Shale Group (Woods et al., 2011), Conasauga Group (Gerhardt and Gill, 2016; LeRoy and Gill, 2019), and Road River Group (Strauss et al., 2020), as well as the DICE in the Alum Shale (Ahlberg et al., 2009), Arthur Creek Formation (Pagès and Schmid, 2016), and Wheeler Shale (Howley and Jiang, 2010).

Samples from the Stockingford Shale Group came from cores from Merevale boreholes −1 (52.561735°N, 1.55977°W) and −3 (52.558636°N, 1.548445°W) and two sections exposed at the Oldbury Quarry (52.551967, 1.544237°W; 52.560985°N, 1.551519°W), all located in the Nuneaton area of Warwickshire, United Kingdom (see Fig. 3 and Woods et al., 2011 for which stratigraphic intervals are captured by these cores and quarry sections). Samples were taken from the cores at regular intervals (approximately every 1.2 m when possible through most of the stratigraphy), marked with respect to original depths in feet, converted to meters, and plotted against the composite stratigraphic section of Woods et al. (2011) (Fig. 3). Samples from the Oldbury Quarry exposures come from the collections of Woods et al. (2011) and were taken every meter in those sections. Note that the Merevale boreholes −1 and −3 were not drilled perpendicular to dip and in Fig. 3 the depths represented by the cores do not represent true stratigraphic thickness (see Woods et al., 2011 for additional details of the orientations of the drill cores in relation to bedding). We chose not to report sample positions corrected to true stratigraphic thickness so as not to potentially misrepresent the placement of our samples in the core and stratigraphy.

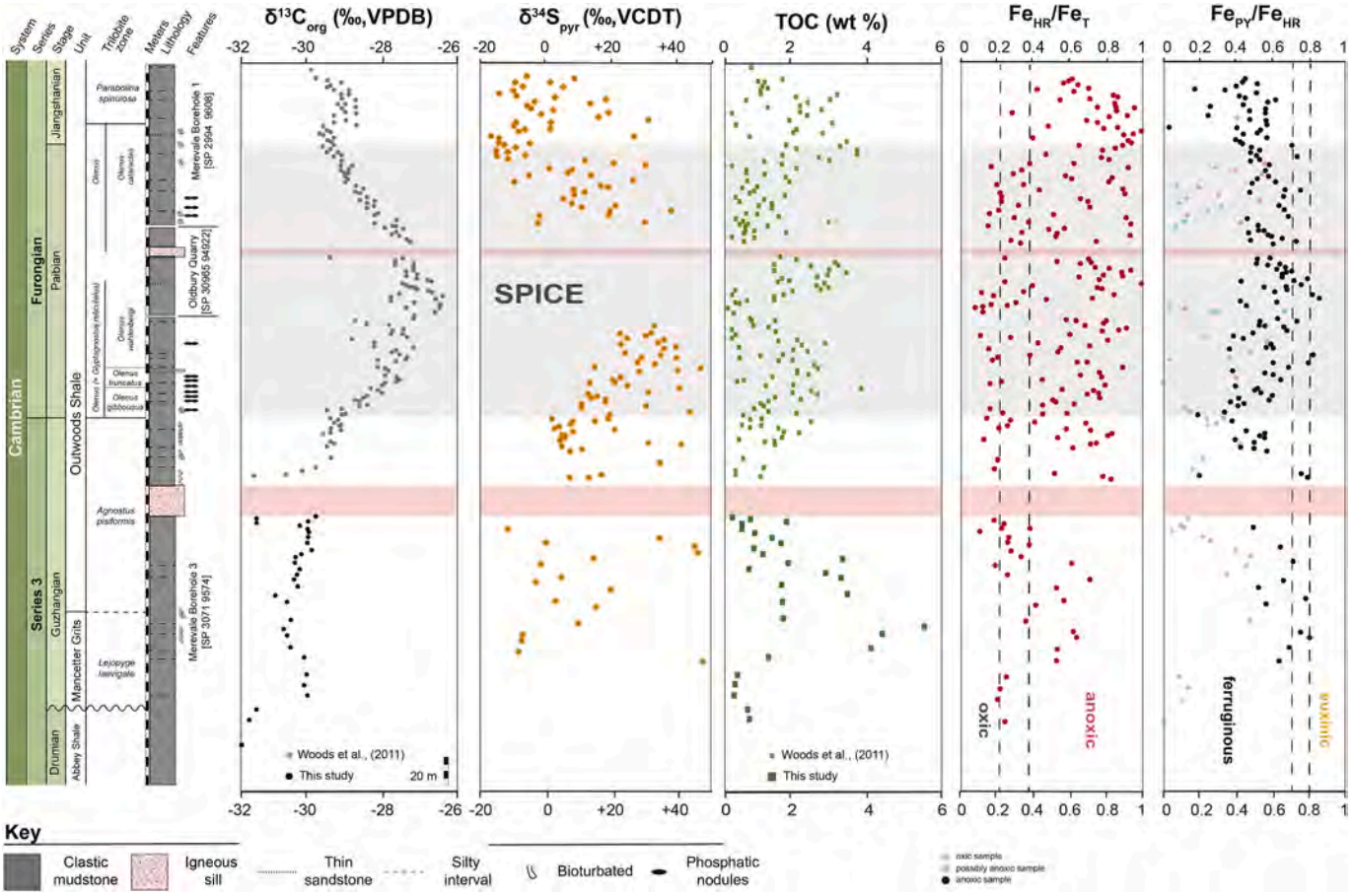

Fig. 3. Stratigraphic column and geochemical data for the Stockingford Shale Group (Nuneaton, U.K). The displayed stratigraphy is a composite section incorporating two boreholes (Merevale-1 and -3) and an outcrop locality (Oldbury Quarry). Note that the thickness for the borehole portion of the composite section represented here is not true stratigraphic thickness because the boreholes were not drilled perpendicular to dip (see Woods et al., 2011 for additional details). Stratigraphic information, TOC (light green squares), and $\delta^{13}C_{org}$ (light gray circles), are from Woods et al. (2011) and references therein. New $\delta^{13}C_{org}$ and TOC data (this study) are displayed as black circles and dark green squares respectively. Gray shaded boxes denote the SPICE interval and the red shaded boxes indicate the stratigraphic level of igneous intrusions. Note that the base of the Oldbury Quarry section is also intruded by an igneous sill that is not depicted here. In the Fe_{Py}/Fe_{HR} plot black dots indicate anoxic samples, pink dots are potentially anoxic and blue dots depict definitively oxic samples based upon Fe_{HR}/Fe_T ratios. For interpretation of the colors used in this figure the reader is referred to the web version of this article. (For interpretation of the references to colour in this figure legend, the reader is referred to the web version of this article.)

We measured $\delta^{34}S$ of pyrite and iron speciation in the bulk sample powders previously analyzed by Woods et al. (2011) in their study of the SPICE in the Outwoods Shale (part of the Stockingford Shale Group). A new set of samples from below the SPICE interval (Paibian) in the Stockingford Shale Group was collected from the Merevale borehole 3 core and analyzed for $\delta^{34}S$ of pyrite and iron speciation, as well as $\delta^{13}C_{org}$ and TOC contents. In all for this study, 199 samples were analyzed for iron speciation, 137 for the $\delta^{34}S$ of pyrite, and 33 for $\delta^{13}C_{org}$ and TOC contents.

A total of 70 samples of the Machari Formation were collected from the Deoksang locality (37.280556°N, 128.377778°E) found in Gangwon Province, South Korea (Fig. 2). Samples were taken at 0.1-m intervals when possible, but the sampling interval was ultimately dictated on the outcrop exposure and the availability of fresh unweathered material. All the Deoksang samples and those from the Stockingford Shale Group not previously crushed were washed in doubly deionized water, disaggregated in a jaw crusher and powdered in a silica nitride SPEX ball mill in the geochemistry lab at Virginia Tech. Sample powders were analyzed for $\delta^{13}C_{carb}$, $\delta^{13}C_{org}$, TOC, $\delta^{34}S$, and iron speciation using the techniques described below.

3.1.1. Total organic carbon contents and carbon isotopic compositions

To determine the total organic carbon content (TOC) and isotopic composition ($\delta^{13}C_{org}$) of our samples, we first removed the carbonate fraction from the bulk sample powders. To achieve this, we reacted between 0.3 and 0.5 g of bulk powder with 2 M HCl for a minimum of 24 h and until no further CO_2 was evolved from the sample. The remaining insoluble residues were then neutralized with doubly deionized water and subsequently dried, reweighed (to determine mass loss) and homogenized. 1 to 10 mg of decarbonated sample powders were then weighed into tin capsules and combusted at 950 °C in an Elementar Vario Cube elemental analyzer connected to an Isoprime 100 CF-GS-IRMS in the stable isotope lab in the Department of Geosciences at Virginia Tech. Samples were run with international and commercial isotopic (CH-6 = −10.449‰; CH-7 = −32.151‰; Elemental Microanalysis wheat flour = −27.21‰) and elemental standards (acetanilide, wheat flour) for calibration to the VPDB scale and to monitor in-run and inter-run precision. The standard deviation (1σ) of the isotopic standards was <±0.1‰. The TOC of each sample was determined using the integrated area of the CO_2 peak measured by the elemental analyzer calibrated to a size series of acetanilide elemental standards. The carbon content of the acetanilide and wheat flour standards calculated using this method averaged less than 5% error from their known compositions. TOC values were corrected using the ratio of the masses of the decarbonated sample to the bulk powder to account for the mass lost during decarbonation.

3.1.2. Pyrite sulfur contents and sulfur isotopes

We extracted pyrite sulfur using the standard chromium reduction of sulfide (CRS) procedure of Canfield et al. (1986). In this study, between 0.1 and 5 g of bulk sample powders were reacted on the specialized distillation line with larger masses used for samples with limited sulfide content. The evolved H_2S gas was passed through a basic solution of zinc acetate and precipitated as zinc sulfide (ZnS) which was later converted to silver sulfide (Ag_2S). The Ag_2S precipitate was vacuum filtered, allowed to dry and then weighed to determine pyrite sulfur contents. Pyrite iron contents were determined assuming a 2:1 stoichiometric relationship between the molar recovery of Ag_2S and the original pyrite (FeS_2) contents of the sample. The dried and weighed precipitate was homogenized using an agate mortar and pestle.

Between 0.350 and 0.450 mg of homogenized Ag_2S precipitate was weighed into tin capsules and combusted at 1050 °C in an Elementar Vario Cube elemental analyzer following the method of Fry et al. (2002). This sample gas was then analyzed by an Isoprime 100 GS-CF-IRMS in the stable isotope lab in the Department of Geosciences at Virginia Tech. Samples were run with international isotopic standards (IAEA S-1 = −0.30‰; IAEA S-2 = 22.7‰; IAEA S-3 = −32.3‰) for calibration to the Vienna Canyon Diablo Troilite (VCDT) scale and to monitor in-run and between-run accuracy and precision. An elemental standard (Elemental Microanalysis sulfanilamide) was also run for calibration of elemental compositions. Reproducibility of the isotopic standards and sample replicates was better than 0.2‰ (1σ) over all analytical runs.

3.2. Iron speciation paleo-redox proxy

Iron speciation analysis has become a common tool for characterizing water-column redox conditions during the deposition of fine-grained siliciclastic sediments throughout the geologic record (Canfield et al., 2008; Jin et al., 2016; Sperling et al., 2015b). Studies of modern marine sediments have demonstrated that enrichments of "highly-reactive iron" (i.e., iron that is reactive towards dissolved sulfide over early diagenetic timescales) are characteristic of sediments deposited under an anoxic water column (Anderson and Raiswell, 2004; Poulton and Raiswell, 2002; Raiswell and Canfield, 1998). Whether a sample is enriched in reactive iron is determined by quantifying the proportion of iron that resides in reactive phases (operationally-defined pools) relative to the total iron content of the sample. Three of these pools are measured using the sequential extraction procedure developed by Poulton and Canfield (2005): iron in carbonate phases (Fe_{Carb}); iron in ferric (oxy)hydroxide phases (Fe_{Ox}); and iron contained in magnetite (Fe_{Mag}). Following the extractions, the concentration of iron in the solutions was quantified by spectrophotometry using the ferrozine method (Stookey, 1970; Viollier et al., 2000) and related to the mass of iron bound in each phase in the original sample. Replicate analyses were reproduced with differences less than 5%. Iron bound as pyrite (Fe_{Py}) is determined using the CRS procedure described above. The sum of the iron content in these four pools defines the highly reactive iron (Fe_{HR}) content of a given sample such that $Fe_{HR} = Fe_{Carb} + Fe_{Ox} + Fe_{Mag} + Fe_{Py}$.

Total iron contents were determined using a modified version of the technique found in Aller et al. (1986). Briefly, sample powders were heated in a muffle furnace at 900 °C for 8 h. These ashed powders were then homogenized, weighed and placed in sealed Savilex vials with concentrated HCl (12 M), and heated on a hot plate set at 145 °C for 48 h. As above, iron concentrations of the supernatant were determined via spectrophotometry using the ferrozine method (Stookey, 1970; Viollier et al., 2000). Replicate analyses were reproduced with differences less than 5%.

Studies of modern and well-characterized ancient environments have established that Fe_{HR}/Fe_T ratios above 0.38 are characteristic of anoxic conditions in the water column and that ratios below 0.22 reflect deposition under oxic bottom waters (Poulton and Canfield, 2011; Poulton and Raiswell, 2002; Raiswell and Canfield, 1998). We note here that 'oxic', as defined in the typical interpretive framework used for the iron speciation proxy, only refers to the presence of oxygen in the water column and not its absolute concentration. Modern sediments deposited under bottom water classified as oxic by their oxygen content (>80 μM O_2) and dysoxic/dysaerobic (5 to 80 μM O_2) display similar ranges of Fe_{HR}/Fe_T (Raiswell et al., 2018; Raiswell and Canfield, 1998). Therefore, these important and biologically relevant differences in bottom water oxygen content (Sperling et al., 2015a) cannot be resolved by the iron speciation proxy. In this study, we will refer to samples with $Fe_{HR}/Fe_T < 0.22$ as oxic, but with the acknowledgement that these samples likely encompass a range of bottom water oxygen contents. Samples with Fe_{HR}/Fe_T ratios between 0.22 and 0.38 are considered 'possibly anoxic' as some modern and ancient sediments deposited under oxic, dysoxic, and anoxic conditions can fall within this range, and therefore Fe_{HR}/Fe_T in this range is ambiguous in delineating the redox state of the water column (Poulton and Canfield, 2011; Raiswell et al., 2018). Anoxic samples can be further classified as being either euxinic (anoxic, with free H_2S in the water column) or ferruginous (anoxic but lacking water-column H_2S) based on the proportion of reactive iron partitioned into pyrite relative to the total pool of available reactive iron (Raiswell and Canfield, 2012). If 70% of the available reactive iron has been pyritized ($Fe_{Py}/Fe_{HR} > 0.7$) this indicates possibly euxinic conditions, while ratios above 0.8 are regarded as definitively euxinic. Conversely, ratios below these thresholds indicate ferruginous conditions (März et al., 2008; Poulton and Canfield, 2011).

The Fe speciation proxy and its interpretive threshold values were originally developed and calibrated using fine-grained siliciclastic sediments from modern marine environments. However, more recent work by Clarkson et al. (2014) has extended the applicability of this proxy to carbonate-rich sediments. These authors demonstrated that such carbonate-rich sediments can still accurately document depositional redox conditions given the important caveat that the total iron content of the samples analyzed exceeds 0.5 wt%. While the vast majority samples considered here come from fine-grained, siliciclastic lithologies, some samples from the Machari Formation have relatively high carbonate contents, and nine had carbonate contents >50%. We therefore used the minimum threshold of 0.5 wt% total Fe to exclude some of the Machari Formation samples from subsequent redox interpretations (see Section 4.2.3 for details about these excluded samples).

4. Results

4.1. Stockingford Shale Group: Nuneaton, U.K

Fig. 3 displays our new Fe speciation, carbon (TOC and $\delta^{13}C_{org}$) and sulfur ($\delta^{34}Spy$) results and the previously reported data (TOC and $\delta^{13}C_{org}$) of Woods et al. (2011) for the rocks of the Stockingford Shale Group in north-central England (Nuneaton, U.K). This composite stratigraphic section includes upper portions of the Abbey Shales, and the entirety of the Mancetter Grits and Outwoods Shale from segments in two boreholes and an outcrop (Merevale-1, Merevale-3 and the Oldbury Quarry, respectively). This composite stratigraphy captures the entire expression of the SPICE event at this location. The numerical geochemical data used to construct Fig. 3 can be found in the Supplementary Material in Table S1.

4.1.1. Bulk organic carbon isotope stratigraphy

Our new $\delta^{13}C_{org}$ data build upon the carbon isotope stratigraphy of Woods et al. (2011) by extending the record through the rest the Outwoods Shale and underlying Mancetter Grits and Abbey Grits/Shales. These new carbon isotopic measurements extend the chemostratigraphic record through the Guzhangian Stage at this location: from the *Lejopyge laevigata* through the *Agnostus pisiformis* trilobite biozones. The lowermost Guzhangian is not represented at this location as the contact between the Mancetter Grits and underlying Abbey Shales is unconformable based upon available biostratigraphic data (Rushton, 1978, 1983). Carbon isotope values ($\delta^{13}C_{org}$) in this portion of the stratigraphy

decrease across the *Lejopyge laevigata* zone (lower Guzhangian) from −30 to −31‰. This trend is reversed across the *Agnostus pisiformis* zone (upper Guzhangian), where $\delta^{13}C_{org}$ slowly rises from around −30.5‰ to −30‰ leading into the initiation of the SPICE near the Guzhangian/Paibian Stage boundary as delineated by Woods et al. (2011). It is important to note the effects of a diabase sill emplaced later in the Paleozoic (Late Ordovician) that is encountered between 90 and 110 m in the Merevale-3 borehole. Woods et al. (2011) attributed $\delta^{13}C_{org}$ anomalously enriched in ^{12}C near this horizon (and several smaller intrusions) to thermal alteration during emplacement and we too find similar effects in our samples in closest proximity below the sill.

4.1.2. Pyrite sulfur isotope stratigraphy

We analyzed the sulfur isotopic composition of 151 sulfide samples prepared from bulk sample powders by the CRS procedure (see Section 3.1.2). We found an overall range of ~70‰ in $\delta^{34}S_{py}$ across the examined stratigraphy with values ranging between about −20‰ to +50‰ (VCDT). Within the pre-SPICE interval that spans the *Lejopyge laevigata* through *Agnostus pisifomis* trilobite biozones (Guzhangian Stage), $\delta^{34}S_{py}$ compositions vary between roughly −10 and +20‰ and lack any discernable directional trend. With the initiation of the rising carbon isotopic values of the SPICE we see a sympathetic rise in $\delta^{34}S_{py}$ across the *Olenus gibbosus* through the *Olenus wahlenbergi* trilobite biozones (Paibian Stage). Here the bulk of the samples rise from values of ~0‰ to about 40‰ at the top of this zone, which also represents the top of the Merevale-3 borehole. While there is a wide scatter in $\delta^{34}S_{py}$ across this portion of the stratigraphy, the overall trend is towards $\delta^{34}S_{py}$ more enriched in ^{34}S coincident with the rise in carbon isotopic values. The strata represented in the Merevale-1 borehole records the falling limb of the SPICE and a second smaller post-SPICE carbon isotope excursion covering the *Olenus wahlenbergi* through *Parabolina spinulosa* trilobite zones (Paibian through Jiangshanian Stages). The overall trend in $\delta^{34}S_{py}$ through this core mirrors that of the carbon isotope record, decreasing from around +30‰ to −20‰ with the falling limb of the SPICE, and fluctuating in conjunction with the second $\delta^{13}C$ peak during the Jiangshanian from −20‰ up to 20‰ before returning to −20‰ at the top of the examined stratigraphic section.

4.1.3. Iron speciation

A total of 199 Stockingford samples were analyzed for Fe speciation with 132 of these samples indicating anoxia ($Fe_{HR}/Fe_T > 0.38$.). The vast majority (114 out of 132; 87%) of these anoxic samples record ferruginous ($Fe_{Py}/Fe_{HR} < 0.7$) rather than euxinic conditions at the time of deposition (Fig. 3). In the pre-SPICE interval spanning the *Lejopyge laevigata* through *Agnostus pisifomis* trilobite biozones (Guzhangian Stage) 23 of 50 (46%) samples indicate anoxic deposition with a mean of 0.43 ± 0.23 overall. Of the 23 anoxic samples in this interval just 6 (26%) indicate the presence of highly reducing euxinic conditions. Within the SPICE interval, which spans the *Olenus gibbosus* through the *Olenus cataractes* trilobite zones (Paibian through lowest Jiangshanian Stages) 80 of 117 (68%) samples indicate anoxia, with a mean Fe_{HR}/Fe_T ratio of 0.56 ± 0.27. Only 12 out of the 80 (15%) anoxic samples within this interval are above the threshold that characteristic euxinia. The post-SPICE interval that spans the *Parabolina spinulosa* trilobite zone (Jiangshanian Stage) has 29 out of 30 (97%) samples with Fe_{HR}/Fe_T ratios indicating anoxia, with an average value of 0.73 ± 0.19 for the interval. All of the samples from this uppermost portion of the examined stratigraphy indicate that anoxic conditions were ferruginous.

4.2. Machari Formation, Deoksang Section, South Korea

We performed the same suite of analyses ($\delta^{13}C_{org}$, $\delta^{13}C_{carb}$, $\delta^{34}S_{py}$ and Fe speciation) on 70 samples of the Machari Formation from the Deoksang locality in South Korea (Sino-Korea). These samples span the *Ptychagnostus sinicus* through *Glyptagnostus reticulatus* trilobite biozones (upper Wuliuan through Paibian Stages) and these geochemical data are displayed in Fig. 4 and available in Table S2 in the supplementary material.

4.2.1. Carbon isotope stratigraphy

The stratigraphy at the Deoksang locality records the SPICE and the DICE in both organic carbon ($\delta^{13}C_{org}$) and carbonate carbon ($\delta^{13}C_{carb}$) isotope records (Fig. 4). The DICE is expressed as an ~−2‰ shift in both $\delta^{13}C_{org}$ and $\delta^{13}C_{carb}$ occurring over the *Ptychagnostus atavus* trilobite zone, that is then followed by a +2‰ return over the *Lejopyge armata* trilobite biozone. In contrast to this, the SPICE is expressed as positive shifts of ~2‰ in $\delta^{13}C_{carb}$ and ~1‰ in $\delta^{13}C_{org}$ over the *Glyptagnostus reticulatus* zone (Paibian Stage). It is important to note that the full expression of the SPICE appears not to be captured in this section, as the available biostratigraphic data indicate that most of trilobite zones of the Paibian Stage are absent at the Deoksang locality.

4.2.2. Pyrite sulfur isotopes

We analyzed the sulfur isotopic composition of the 35 Machari samples that yielded enough sulfide for isotopic analysis. Overall, there is a range of around 60‰ in $\delta^{34}S$ (between −10 and +50‰ VCDT) through the approximately 10 m of stratigraphy examined. The lowest values are encountered in the *Ptychagnostus atavus* biozone. $\delta^{34}S$ is highly variable in this zone and becomes less variable and more positive up section into the *Lejopyge armata* biozone in conjunction with the rise in carbon isotopes at the end of the DICE. In contrast to the paired carbon and sulfur isotopic trends we observe during the Drumian, across the Paibian Stage values are scattered around +30‰ and lack any clear directional trend despite the rise in carbon isotopes indicating the SPICE (Fig. 4).

4.2.3. Iron speciation

Of the 70 samples from the Machari Formation that we analyzed for Fe-speciation, we have excluded 21 from our interpretations of local redox since they have total Fe contents below 0.5 wt%, a threshold below which the proxy has been shown to be unreliable in carbonate sediments (Clarkson et al., 2014; Raiswell et al., 2018; see Section 3.2 for details). Of the remaining 49 included samples, 45 indicate anoxia (92%), three indicate possible anoxia and only one suggests oxic depositional conditions (see Section 3.2 for information about interpretive thresholds). Overall these 49 samples have a mean Fe_{HR}/Fe_T ratio of 0.56 ± 0.14, and all but two (43 total; 88%) display Fe_{Py}/Fe_{HR} ratios indicative of ferruginous rather than euxinic conditions.

5. Discussion

5.1. Fidelity of the new geochemical records

5.1.1. Iron speciation

A fundamental concern when using the Fe-speciation proxy to reconstruct ancient bottom-water oxygenation is determining whether the signals encoded in the rocks are primary in origin, i.e., unaffected by any significant post-depositional diagenetic alteration. We are confident that the vast majority of the new analyses from the Stockingford Shale Group and the Machari Formation that we report here faithfully record primary depositional signals for several reasons. Raiswell et al. (2018) outlined several important guidelines to consider when assessing the fidelity of iron proxy data including: the use of fresh un-weathered material, exclusion of samples subjected to extensive alteration by metamorphism or interaction with post-depositional fluids, and excluding samples with low TOC and Fe_T (< 0.5 wt%). The Stockingford and Machari samples we analyzed generally meet all of these screening requirements (except for 21 Machari samples excluded based on low Fe_T content, see Section 4.2.3 for details). However, some further pertinent details about the sedimentology and post-depositional history of these two units bear mentioning. The Stockingford strata are intruded by several diabase sills during the early Paleozoic (Late Ordovician). Their

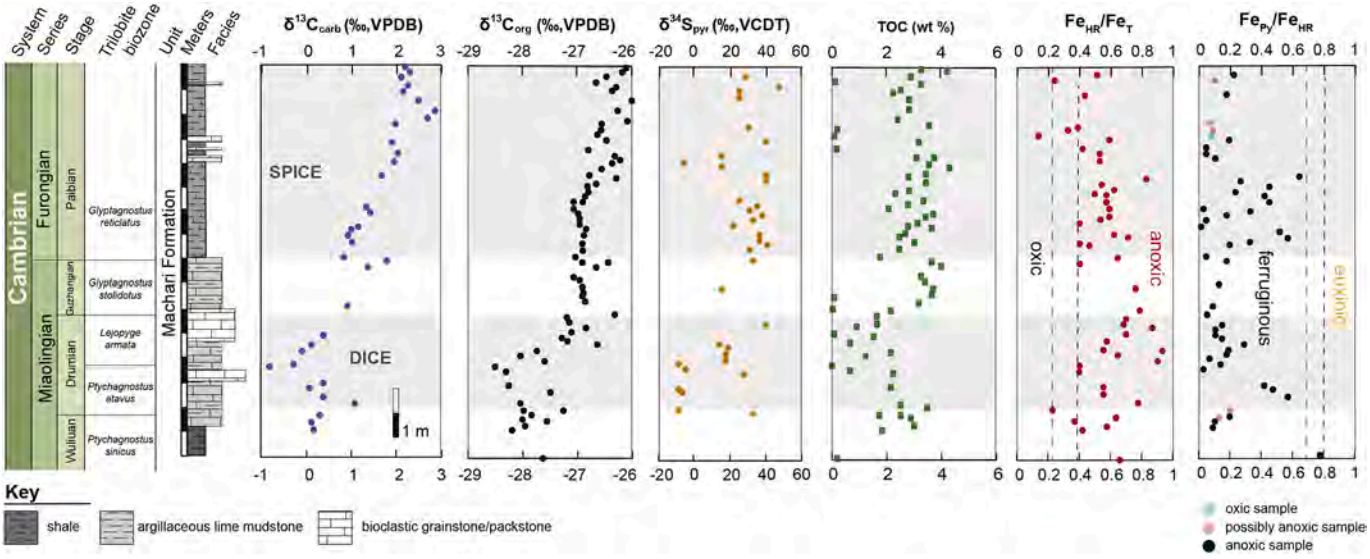

Fig. 4. Stratigraphic details and geochemical data for the Deoksang section of the Machari Formation (South Korea). Gray shaded boxes indicate the stratigraphic level of the DICE and SPICE isotope excursions respectively. Note, only the beginning of the SPICE excursion is represented in this section; the section is terminated by a fault at the top. See Choi et al. (2016) and references therein for further details about this stratigraphic section. As in Fig. 3 black dots in the Fe_{Py}/Fe_{HR} plot indicate anoxic samples, pink dots are potentially anoxic and blue dots depict oxic samples based on Fe_{HR}/Fe_T ratios. (For interpretation of the references to colour in this figure legend, the reader is referred to the web version of this article.)

emplacement may have mobilized late-stage diagenetic fluids, volatilized S and C or otherwise altered Fe-mineralogy (e.g., incorporation of reactive iron in sheet silicates) of the sediments proximal to these igneous bodies. Despite these potential complications we see no pattern of systematic changes in our iron data from the samples adjacent to these bodies, either in terms of total iron content or the distribution of iron between the various pools of highly-reactive iron (see supplementary material Table S1) as would be expected from such processes, bolstering our confidence that any effects experienced in this regard were negligible.

While all efforts were made to collect and analyze visibly unweathered samples, some of the Machari samples may have been subjected to oxidation, possibly leading to the conversion of pyrite to iron oxide minerals. Of the 49 Machari samples included in our analysis, we record 17 that display both anomalously high Fe_{ox} and low Fe_{py} values (see Table S2). If pyrite oxidation is responsible for the pattern of iron partitioning in these samples, the interpretations of redox based on Fe_{HR}/Fe_T values would nonetheless remain unaffected, as iron oxidized from pyrite by this process would still be quantified in the highly-reactive pool during the sequential extraction procedure. This process would however lower Fe_{Py}/Fe_{HR} values and potentially obscure a signal of euxinia by mischaracterizing how iron was originally partitioned between the different reactive phases. In light of this, we consider the extreme case where all the iron liberated during the sodium dithionite (iron oxide pool) extraction performed on these samples was originally present as pyrite prior to oxidation. In this scenario we find that conditions would have been considerably more reducing, with all 12 of the definitely anoxic samples ($Fe_{HR}/Fe_T > 0.38$) shifted to Fe_{Py}/Fe_{HR} values between 0.7 and 0.8 or >0.8, thereby indicating possibly euxinic and definitely euxinic conditions for roughly a third of the Machari samples. Interestingly, it is notable that most of these samples fall within the DICE and SPICE intervals (see Fig. S3 for a data plot based on this assumption) which are thought to be associated with transient increases of euxinia in portions of the oceans (e.g. Dahl et al., 2014; Gill et al., 2011; Pagès et al., 2016).

Finally, Slotznick et al. (2020) has recently noted that the oxalate step in the sequential iron extraction can also potentially dissolve Fe-bearing clays, leading to an overestimation of the highly reactive iron pool. However, all Stockingford and Machari samples contain negligible oxalate extractible iron contents (supplementary material Tables S1 and S2). This suggests if Fe-bearing clays are present in these samples, they have not substantially contributed to the extracted highly reactive iron pool and subsequently influenced our redox interpretations.

5.1.2. Carbon ($\delta^{13}C_{org}$) and sulfur ($\delta^{34}S_{py}$) isotopic signals

Our carbon isotopic data from the Guzhangian portion of the Stockingford Shale Group appear to faithfully record a primary oceanographic signal and are likely unaffected by any significant post-depositional or diagenetic processes. The overall trend and isotopic values of the $\delta^{13}C_{org}$ profile is consistent with those seen over the same interval in the Alum Shale (see Fig. 4 in Ahlberg et al. (2009) for comparison). Furthermore, this record is also in agreement with numerous $\delta^{13}C_{carb}$ records that span the Guzhangian—a stage characterized by limited isotopic variability that contrasts with the wide swings recorded in most other Cambrian stages (see Fig. 1 in Babcock et al., 2015). We do however observe similar effects as Woods et al. (2011) for several samples that are shifted towards isotopically lighter values near intruding diabase sills. However, these thermally altered samples are easily identified and clearly do not represent isotopic changes to the marine DIC pool or biological fractionation imparted during the generation of organic matter (see Fig. 3) and are therefore disregarded.

Our $\delta^{34}S_{py}$ profiles from sedimentary pyrite in the Stockingford Shale Group, and to a lesser extent the Machari Formation, display differences in the variability and overall range of $\delta^{34}S_{py}$ when compared to the Alum Shale. Pyrite in the Alum Shale (Fig. 3-BL, Gill et al., 2011) records a positive excursion in $\delta^{34}S_{py}$ coincident with SPICE: $\delta^{34}S_{py}$ starts at a Guzhangian baseline that fluctuates around 0 ± 5‰, which is followed by a smooth rise in $\delta^{34}S$ to ~ 20‰ in the Paibian and then a relatively steady decline into the lowermost Jiangshanian to values of ~ −10‰. This overall trend in $\delta^{34}S_{py}$ tracks the positive excursion observed in the $\delta^{34}S$ of seawater sulfate (Gill et al., 2007, 2011; Wotte and Strauss, 2015) that has been attributed to a perturbation in the global sulfur cycle caused by the enhanced burial of pyrite in marine sediments during the SPICE (Dahl et al., 2014; Gill et al., 2007, 2011). While the pyrite in the Stockingford Shale Group (Fig. 3) also broadly records an overall positive $\delta^{34}S_{py}$ excursion with the SPICE, it notably displays considerable (10s of ‰) higher order variation superimposed on this stratigraphic trend.

To understand the differences between the Alum Shale and Stockingford Shale Group $\delta^{34}S_{py}$ records, we need to consider factors that can influence the $\delta^{34}S$ of sedimentary pyrite. The sulfur in sedimentary pyrite is sourced from seawater sulfate which is reduced by microbial sulfate reduction (MSR) to form hydrogen sulfide. This sulfide then reacts with iron-bearing minerals or aqueous ferrous iron, either in the water column or sediment, to produce pyrite. MSR, and subsequent microbial reactions such as disproportionation, can produce sulfide that is depleted in ^{34}S relative to the parent sulfate by up to ~80‰ (e.g. Detmers et al., 2001; Habicht and Canfield, 1997, 2001; Sim et al., 2011a, 2011b). The $\delta^{34}S$ of sulfide, and the pyrite ultimately formed from it, can also be influenced by additional factors. The local sulfate and product sulfide pools can become more ^{34}S enriched when the consumption of sulfate via MSR outpaces its delivery from the water column to zone of sulfate reduction. This causes sulfate limitation and the isotope systematics of sulfur pools to tend towards more Rayleigh type distillation or closed-system behavior (e.g. Pasquier et al., 2017). This can occur when the zone of sulfate reduction moves from the water column into the sediment and/or deeper into the sediment pile and can be caused by increasing sedimentation rates or oxygenation of the bottom waters. The oxidation of sulfide can also influence the $\delta^{34}S$ of the sulfide pool, as abiotic and microbial sulfide oxidation produces oxidized species of sulfur that are depleted in ^{34}S by 4 to 18‰ relative to the parent sulfide (Fry et al., 1984, 1986, 1988; Kaplan and Rittenberg, 1964). The amount of sulfide oxidation that occurs can be influenced by the degree of bottom water oxygenation and also by bioturbation or other physical processes that rework and deliver oxidants into the sediment (e.g. Aller et al., 2010; Ries et al., 2009).

These differences between the smooth $\delta^{34}S_{py}$ trend from the Alum Shale and the highly variable record of the Stockingford Shale Group can be attributed to differences in both sedimentation rate and water column redox conditions during the deposition of these units. Differences in the gross sedimentation rate of these two units is made clear by comparing the thicknesses of the Guzhangian and Paibian Stages: these stages in the Stockingford Shale Group are ten times thicker than in the Alum. These relatively higher sedimentation rates would have favored higher degrees sulfate limitation in the pore waters and the production of a sulfide pool more enriched in ^{34}S. Further, Fe-speciation data from the Stockingford Shale Group indicate that bottom water redox was also highly variable over the study interval and varied between oxic, ferruginous, and euxinic conditions (Fig. 3 and discussed below). This interpretation for bottom water redox conditions is further supported by the sedimentology of this unit, which is also highly variable and alternates between intervals of dark, laminated mudstones and light-colored mudstones that contain variable degrees of bioturbation (Taylor and Rushton, 1971). These fluctuating redox conditions produced a highly variable $\delta^{34}S_{py}$ record through frequent changes in depth of the zone of MSR, which in turn dictated the extent of sulfate limitation, and also the intensity of sulfide oxidation through controlling the availability and delivery of oxidants. In contrast, the Alum was deposited under more persistently stable anoxic conditions (Gill et al., 2011) where the zone of MSR was either located in the water column or near the sediment-water interface. This resulted in a much less variable $\delta^{34}S_{py}$ record that more closely followed the $\delta^{34}S$ of the marine sulfate reservoir.

Despite the large stratigraphic variability in $\delta^{34}S$ of the Stockingford Shale Group, we still observe an overall positive $\delta^{34}S$ excursion that likely reflects the change in the isotopic composition of the marine sulfate reservoir. Notably, over the lower Paibian we observe a distinct positive shift in $\delta^{34}S_{py}$, coupled with rising $\delta^{13}C_{org}$ values that are followed by a decline in both $\delta^{13}C$ and $\delta^{34}S_{py}$ in the upper Paibian and remains paired to changes in $\delta^{13}C$ through the lower Jiangshanian. This paired pattern is consistent with findings from other successions globally that record the SPICE and further supports the primary oceanographic nature of these signals; given that these trends remain conspicuous despite second-order variability likely caused by local sedimentary and diagenetic processes like those discussed above.

5.2. Redox trends during the middle to later Cambrian

In addition to the new geochemical records from Avalonia and the Sino-Korean Block, as mentioned above, this study also considers previously published iron speciation data from Baltica (Gill et al., 2011), Laurentia (LeRoy and Gill, 2019; Sperling et al., 2015b; SGP data), and Gondwana (Creveling et al., 2014). We use these combined datasets to compare how different environmental parameters influenced local redox conditions at each location with the goal of elucidating broader patterns about the redox structure of middle to late Cambrian oceans. Most strikingly and perhaps not surprisingly, when comparing the study sites relative water depth (basinal position) is the most important determinant of the prevailing redox environment. Specifically, our data reveal outer shelf and basinal environments (Fig. 5C) to have been dominantly anoxic ($Fe_{HR}/Fe_T > 0.38$), and inner shelf environments (Fig. 5E) were largely devoid of definitively anoxic conditions ($Fe_{HR}/Fe_T < 0.38$).

Given these observations, we begin by outlining the broad similarities and differences we observe within and between these two groups of environments (Sections 5.2.1 and 5.2.2). Next, we consider sampling biases that might limit the accurate characterization of global trends in oceanic redox structure (Section 5.3). Finally, we look at the relationship between the redox trends revealed in our data and the broader co-evolution of the biosphere and ocean-atmosphere system during the early Paleozoic (Section 5.4).

5.2.1. Outer shelf and basinal environments

Six of the seven successions that we examined (those from Sino-Korean Block, Baltica, Australia, North Laurentia, and Avalonia) provide records of conditions in relatively deep-water, outer shelf and basinal environments. Based on the Fe-speciation data, these environments appear to have been predominantly anoxic throughout the middle to later Cambrian study interval. Overall, these six locations record anoxic conditions in 64% (317 of 497) of samples, with ferruginous bottom waters significantly more common (54%, 268 samples) than euxinic (10%, 49 samples). Definitively oxic conditions were apparently quite rare in these environments as only 15% (75 of 497) of our samples have $Fe_{HR}/Fe_T < 0.22$ (Fig. 5C). Binning the outer shelf and basinal data at the stage level we find that 75% of Wuliuan samples (3 of 4), 43% of Drumian (87 of 201), 71% of Guzhangian (48 of 68), 78% of Paibian (158 of 203), and all the Jiangshanian samples (21) had $Fe_{HR}/Fe_T > 0.38$ indicating anoxic water columns during deposition (Fig. 5D). Among these samples euxinic conditions were only a substantial portion of the anoxic sample population in the Guzhangian (31%) and Paibian (20%). These stages stand in contrast to the Wuliuan, Drumian and Jiangshanian where euxinia was indicated in only three out of the 217 anoxic samples.

While these six locations are all interpreted as outer shelf/basinal environments, they nonetheless each represent unique local conditions in terms of sedimentation rates, changes in local sea level and organic matter and sulfate availability. Each of these factors would be expected to have influenced the preserved geochemical signals. The most important difference we recognize between these sites is the stratigraphic thickness of each stage at each location, and by extension sedimentation rate. The Stockingford, Wheeler, Road River, and Arthur Creek successions have thicknesses of hundreds of meters while the equivalent intervals in the Alum and Machari are significantly thinner at only tens of meters or less. These differences in sedimentation would have affected several processes that would have had the potential to influence local redox by increasing or decreasing: (i) the exposure time of organic matter to oxidative degradation; (ii) the remobilization of nutrients from sediments, which is an important positive feedback that can sustain seafloor anoxia (Ingall and Jahnke, 1994); (iii) the concentration and availability of organic matter and bioturbation intensity; (iv) supply of seawater sulfate into the zone of MSR within the sediment versus the supply of reactive iron minerals available to titrate sulfide

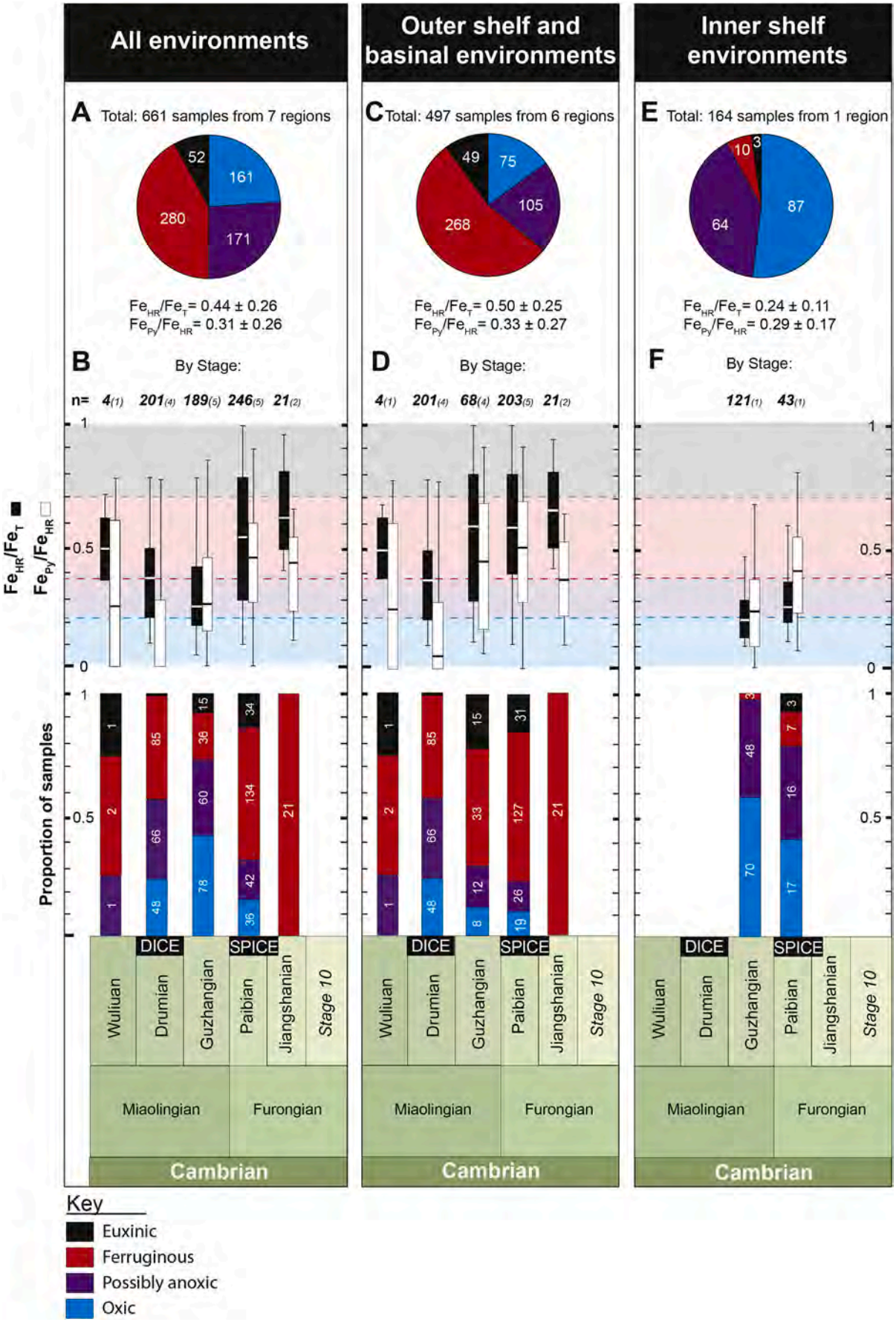

(caption on next page)

Fig. 5. Combined iron speciation results from Avalonia, Sino-Korea Block (both this study), Baltica (Gill et al., 2011), Laurentia (LeRoy and Gill, 2019; Sperling et al., 2015b; SGP data) and Australia (Creveling et al., 2014). The proportion of samples indicating oxic (blue), possibly anoxic (purple), and anoxic (red-ferruginous; black-euxinic) conditions are displayed as totals (pie charts) and binned by geologic stage (bar charts in lower panels). Numbering within charts indicates the number of samples comprising each respective category. Panels A & B show results for all samples combined, C & D show the subset from outer shelf and basinal environments, and E & F show the subset from inner shelf environments. Box and whisker plots in each middle panel display the interquartile range (Q2-Q3, box), median (solid line within boxes) and 1.5 times the interquartile range (whiskers) for Fe_{HR}/Fe_T (black boxes) and Fe_{Py}/Fe_{HR} (white boxes) data binned by stage. Shading in these plots corresponds to the redox interpretation colour scheme used throughout this figure. The reader is referred to Section 3.3 for the Fe_{HR}/Fe_T and Fe_{Py}/Fe_{HR} threshold values used for all redox interpretation assignments. (For interpretation of the references to colour in this figure legend, the reader is referred to the web version of this article.)

generated by MSR, potentially modulating the development of euxinic conditions.

Our iron speciation results bear out differences between the compared outer shelf and basinal environments that are broadly consistent with the expected influence of sedimentation rate on these processes. Specifically, we find that the greater stratigraphic thicknesses of the Arthur Creek and Wheeler formations and the Stockingford and Road River groups generally record less-reducing conditions (lower Fe_{HR}/Fe_T, Fe_{Py}/Fe_{HR}), lower TOC and S_{py} contents relative to the equivalent intervals in the stratigraphically condensed Alum and Machari Formations (Table 1). In fact, with the exception of the Alum (and potentially the Machari for reasons outlined in Section 5.1.1) none of the other outer shelf and basinal environments record any prolonged interval of euxinic conditions.

These differences illustrate the control that organic carbon, iron and sulfate availability exert in driving a system either towards ferruginous or euxinic conditions as explored in Johnston et al. (2010). In particular, the data compared here suggest that the balance of these controls favored ferruginous conditions during this interval. In many of these deeper-water environments the supply of organic carbon was apparently sufficient to drive iron reduction and reduced iron accumulation but insufficient for the generation of enough free hydrogen sulfide to accumulate in sedimentary pore waters and subsequently in the water column. Sulfide production would have also been inhibited at locations with relatively high sedimentation rates where sulfate supply to the sedimentary porewaters would have been limited. Moreover, estimates for the marine sulfate pool in the middle to later Cambrian suggest that it was much small than the modern (Brennan et al., 2004; Gill et al., 2007), making the conditions under which sulfate limitation could occur more common. Overall this suggests that these environments were largely ferruginous as a result of relatively low organic matter production and availability, and to a lesser extent sulfate availability as dictated by

Table 1
Stage-level stratigraphic and geochemical features of the seven Cambrian successions compared in this study. All geochemical data represent mean values (±1σ) of a given parameter for each stage by location. Total iron (Fe_T), total organic carbon (TOC) and pyrite sulfur (Spy) are all reported as wt%. Note that the thickness for the Stockingford Shale Group listed here are true stratigraphic thickness.

Stage	Thickness (m)	FeHR/FeT	FePy/FeHR	FeT	TOC	Spy	$\delta^{34}S_{pyr}$
Alum							
Drumian	6	0.75 ± 0.08	0.67 ± 0.06	4.4	4.6	2.2	0.1
Guzhangian	10	0.94 ± 0.08	0.77 ± 0.09	4.9	7.9	4.1	2.8
Paibian	10	0.82 ± 0.12	0.83 ± 0.05	5.8	12	4.5	7.7
Jiangshanian							
Arthur Creek							
Drumian	150	0.46 ± 0.14	0.47 ± 0.15	1.61	0.41	0.45	
Guzhangian							
Paibian							
Jiangshanian							
Conasauga							
Drumian							
Guzhangian	100	0.22 ± 0.07	0.22 ± 0.08	2.99	0.15	0.16	3.3
Paibian	30[a]	0.29 ± 0.16	0.29 ± 0.17	2.43	0.2	0.3	37.9
Jiangshanian							
Machari							
Drumian	2	0.62 ± 0.21	0.23 ± 0.16	1	1.7	0.12	10.6
Guzhangian	1	0.70 ± 0.18	0.11 ± 0.05	0.57	2.7	0.14	14.8
Paibian	4[a]	0.51 ± 0.15	0.23 ± 0.19	1.16	2.7	0.11	30.1
Jiangshanian							
Road River							
Drumian							
Guzhangian	60[a]	0.73 ± 0.16	0.30 ± 0.13	1.1	1.4	0.3	
Paibian	90	0.64 ± 0.15	0.30 ± 0.19	1.4	2.1	0.4	
Jiangshanian	14[a]	0.49 ± 0.05	0.18 ± 0.05	1	1.8	0.1	
Stockingford							
Drumian	23[a]						
Guzhangian	125	0.43 ± 0.22	0.44 ± 0.23	5.4	1.4	1.3	12.5
Paibian	103	0.57 ± 0.27	0.47 ± 0.20	5.4	1.5	2.1	14
Jiangshanian	14[a]	0.71 ± 0.15	0.45 ± 0.12	5	1.7	1.8	−1.8
Wheeler							
Drumian	300	0.31 ± 0.17	0.03 ± 0.04	3.2	0.2	0.02	23
Guzhangian							
Paibian							
Jiangshanian							

[a] indicate that the full thickness was not measured or known at that location.

sedimentation rates in a low-sulfate ocean. Under these conditions euxinia was limited to regions of high surface ocean productivity and relatively low sedimentation. This redox structure is similar to that envisioned for portions of the Neoproterozoic (Li et al., 2010) and suggests this redox structure persisted well into the Cambrian and perhaps beyond.

5.2.2. Inner shelf environments

The iron speciation records from the only datasets available from inner-shelf environments presented in LeRoy and Gill (2019) differ quite markedly from the records seen in the other basins described above. This study documented that non-anoxic conditions ($Fe_{HR}/Fe_T < 0.38$) prevailed in the inner-shelf environments at three locations along the southern Laurentian margin during the late Cambrian (Guzhangian into Paibian Stages). In fact, definitively anoxic samples comprise only 8% of samples (13 of 164) from this interval (Fig. 5E), a finding in marked contrast to the deeper-water environments described above. However, when these data are binned at the stage level, differences in the percentage of anoxic samples between the Guzhangian (2%, 3 of 131) and the Paibian (23%, 10 of 43) become apparent (Fig. 5F). This record of increased anoxia in inner shelf environments during the Paibian, the stage encompassing the SPICE event, supports the hypothesis that reducing conditions expanded during this time generally, and that this expansion may have occurred largely and most impactfully in shallow-shelf environments. A deoxygenation of portions of the shallow continental shelves, such a suggested by these data, would have placed severe environmental stress on marine communities in such environments.

5.3. Data limitations

It must be noted that the temporal range represented by the seven successions we examined are not entirely equivalent. For example, the study of LeRoy and Gill (2019) spans only the Upper Guzhangian and lowest part of the Paibian rather than the entirety of either stage. This could be potentially problematic for attempting to identify the redox trends representative of these stages in southern Laurentia. Moreover, these inner shelf datasets are from three locations from the same ocean margin. This clearly limits our broader understanding of environmental change in inner-shelf environments during this time. However, despite the limitations imposed by the temporal and geographic range of the data compilation considered here, we remain confident that valuable information can be extracted from the comparisons made here.

The Fe-speciation records presented in LeRoy and Gill (2019) show remarkably little variability in Fe_{HR}/Fe_T across the Guzhangian portion of the studied stratigraphy. This feature, when viewed in conjunction with contemporaneous C- and S- isotope profiles which are largely invariant (see Figs 4, 5, and 6 in LeRoy and Gill, 2019), suggests a period of relative environmental stability along the southern margin of Laurentia during the Guzhangian. In light of this, we feel these Fe-speciation data are representative of the prevailing conditions in this environment prior to the shift to more reducing conditions that accompanied the SPICE onset (early Paibian) at this location (see Fig. 5F). What remains less clear is what conditions were like over the later portions of the Paibian in inner shelf environments. For example, did anoxia become more or less prevalent or intense (euxinic?) over the course of the SPICE? Unfortunately, this important question remains unresolved as locally in southern Laurentia the depositional environment transitions into a thick shallow water carbonate sequence in the lower Paibian Stage, precluding the use of the Fe-speciation proxy.

Our samples from the Machari Formation share similar temporal limitations as the Laurentian samples described above. The Guzhangian within the Deoksang section is represented by a very thin stratigraphic interval (~1 m) and a limited number of samples (5)—significantly fewer samples and less stratigraphic thickness compared to this interval at the other locations. Additionally, as with the locations in southern Laurentia, only the lowermost Paibian is recorded in the Machari (based on the available trilobite biostratigraphic data) whereas the entirety of this stage is captured in the data from Baltica (Gill et al., 2011) and Avalonia (Stockingford Shale Group, this study). Despite this temporal incongruence, we still remain confident that our data from these Stages within the Machari are representative of the prevailing conditions at the location during the late Cambrian—that is to say that anoxic conditions were apparently a ubiquitous feature of this environment at the time, despite our noted uncertainty (see Section 5.1.1) about its character (ferruginous vs. euxinic).

The limitations in the temporal and geographic range and resolution of the data we present here highlights the need for continued, detailed paleoredox investigations of middle and upper Cambrian strata. In particular, future work focused on expanding redox proxy records beyond the relatively well-documented SPICE interval is necessary to better understand long-term trends and possible secular changes to the "background" state of the Cambrian ocean outside of the numerous carbon cycle perturbations that, to date, have received the bulk of investigative attention. This work will need to rely on a combination of new and traditional paleoredox indicators suited to both shales (Fe-speciation, Mo and Tl isotopes: e.g., Kendall et al., 2017; Owens, 2019), trace metals (e.g., Gill et al., 2011) and in particular to carbonates (I/Ca ratios: e.g., Edwards et al., 2018), U isotopes: e.g., Dahl et al., 2014) as these are the dominant lithology in many successions of this age (see Fig. 2 in Harper et al. (2019) for a generalized facies map for this time).

5.4. Evolutionary implications of Cambrian redox trends

A great deal of research has focused on a possible co-evolutionary relationship between surface oxygen levels and the early diversification of complex metazoan life during the late Neoproterozoic through early Paleozoic (e.g., Canfield et al., 2007; Chen et al., 2015; Lenton et al., 2014; Och and Shields-Zhou, 2012; Sperling et al., 2015b, 2013; Wood and Erwin, 2018). Despite these efforts, debate remains regarding the extent to which these changes in the biosphere were driven by environmental versus biological factors (Cole et al., 2020). Many studies suggest a direct link between increases in the oxygenation of the oceans and atmosphere and the evolutionary expansion of metazoans during this time (e.g. Canfield et al., 2007; Planavsky et al., 2014). Others advocate for a more nuanced relationship between the rise in oxygen and animal evolution (e.g. Mills et al., 2014; Mills and Canfield, 2014; Sperling et al., 2013), specifically noting that oxygen changes differentially affect animal clades and ecologies. Alternatively, it has been argued that metazoan evolution instead drove ocean–atmosphere oxygenation (Butterfield, 2009). The temporal range of our data record allows us to investigate the dynamics of marine anoxia and oxygenation in regards to this broad evolutionary backdrop during a portion of this critical time in the development of animal life. Furthermore, because this time interval also contains two significant carbon-cycle perturbations (SPICE and DICE) it provides the opportunity to evaluate the relationship between these events, changes in nature of the spatiotemporal redox structure of the oceans, and the evolution of early animal ecosystems.

The middle Cambrian to Early Ordovician is characterized by abnormally high rates of turnover in marine fauna (Bambach et al., 2004; Harper et al., 2019). On the finer temporal scale, this turnover is manifested as a series of repeating extinction and diversification events (i.e., the "biomeres" as defined in Palmer, 1965 and Palmer, 1984). Turnover events are associated with the beginning of the SPICE and base of the Paibian Stage (Ahlberg et al., 2009; Eriksson and Terfelt, 2007; Gerhardt and Gill, 2016; Park and Choi, 2011; Peng et al., 2004; Saltzman et al., 1998; Saltzman et al., 2000; Smith et al., 2020) and potentially the DICE (Sundberg, 1994, 1991; Taylor et al., 2012; Williams et al., 2011) though further detailed studies are needed to confirm this relationship for the latter. In the case of the event associated with the SPICE (and the subsequent events in the later Cambrian and Early Ordovician), the biological changes involve an extinction of diverse

shallow-shelf fauna (mainly benthic trilobites and brachiopods), and their replacement by low-diversity faunas typically found in deeper water facies (Freeman et al., 2018; Palmer, 1984, 1965; Rieboldt, 2005; Taylor, 2006). Where turnover has been observed during these events it was apparently more severe for the fauna in shallower shelf environments (Ludvigsen, 1982; Westrop and Ludvigsen, 1987; Woods et al., 2011).

Various mechanisms such as ocean circulation, temperature and oceanic redox have been explored as potential contributors to these observed faunal changes (Babcock et al., 2015; Elrick et al., 2011; Gill et al., 2011; Perfetta et al., 1999; Saltzman et al., 2015; Stitt, 1975). Since our Fe-speciation data suggest that deep-water environments were commonly anoxic across the studied interval, we propose shoaling of these anoxic deep waters onto the shallow shelf either due to sea-level rise or increased nutrient loading followed by subsequent increases in primary productivity and oxygen demand in deeper waters. Expansion of anoxic, and potentially in places euxinic, waters on to shallow shelves could act as direct extinction mechanism, but also, an indirect mechanism through the loss of well-oxygenated shelf area that increased competition for the remaining habitable areas. Overall, this scenario is generally consistent with known ecological patterns associated with this extinction and the geochemical data presented here and elsewhere (Dahl et al., 2014; Gill et al., 2011, 2007). Specifically, Fe-speciation data from inner shelf facies from the southern margin of Laurentia indicate the appearance of anoxic and in some cases euxinic conditions (LeRoy and Gill, 2019) during and immediately after the interval that contains the beginning of the SPICE and extinction event in shallow shelf ecosystems (Cuggy, 1996; Gerhardt and Gill, 2016).

Lower diversity, deeper water ecosystems, like those found in Baltica and Avalonia successions, experienced significantly lower turnover during this event (e.g. Woods et al., 2011). Morphological features of trilobites and other organisms that compose this assemblage suggest that they were adapted to low oxygen conditions (Clarkson and Taylor, 1995; Clarkson, 2011; Fortey, 2000, 1985; Fortey and Wilmot, 1991; Williams et al., 2011) found in the oxygenated edge of the chemocline adjacent to anoxic waters in deeper water environments. Further, as anoxic waters expanded on the shallow shelf, zones of poorly-oxygenated bottom waters would have expanded as well. The deeper-water fauna adapted to these low-oxygen conditions would then be able to colonize areas of the shelf covered by these environments, replacing the extirpated or extinct shallow-water benthic faunal assemblages that were unable to persist there due to their greater oxygen requirements. After the extinction event, as oxygen availability later increased in these shelf environments, the fauna there were able to re-diversify into available ecological niches until ultimately anoxic waters once again bathed the shelves and the process was repeated (Fortey, 1989; Loch et al., 1993; Palmer, 1984).

Interestingly, a somewhat similar evolutionary pattern to that seen in the Cambrian has been observed during portions of the Mesozoic when deeper-water environments are thought to have been similarly deoxygenated. It has been proposed that the expansion and contraction of dysoxic and anoxic conditions into nearer shore environments was likely an important driver of similar evolutionary dynamics and ecological changes seen across Oceanic Anoxic Events (e.g. Harries and Little, 1999). Further, Wood and Erwin (2018) suggest that unstable redox conditions in the early Paleozoic were not only a driver of extinction, but also a critical driver of evolutionary innovation. Both views provide support to the argument that the unique evolutionary dynamics of the early Paleozoic were intrinsically tied to the nature of oceanic redox and fluctuations in its spatiotemporal structure. Thus, our data presented here support this view that deep water anoxia and its expansion (SPICE and DICE) and contraction on shallow shelves may have provided the environmental driving force for *both* high rates of extinction and origination during the middle to later Cambrian and into the Early Ordovician. Only once the frequency and intensity of these anoxic shoaling episodes lessened into the Ordovician was the stage was set for a more stable nearshore environment that eventually fostered the rapid and sustained diversification of the GOBE (Saltzman et al., 2015).

6. Conclusions

The role of marine oxygen availability in the evolution of the biosphere during the late Neoproterozoic and early Paleozoic has been intensively investigated, yet the details of feedbacks within this relationship are still emerging. In this study we explore the link between oceanic redox and evolutionary dynamics across the middle to later Cambrian (Drumian-Jiangshanian Ages)—a key interval between the rapid diversifications of the Cambrian Explosion and GOBE. We present two new geochemical data sets that incorporate $\delta^{13}C_{org}$, $\delta^{34}S_{py}$ and Fe-speciation analyses to characterize redox conditions in basins from Avalonia (Stockingford Shale Group, U·K) and the Sino-Korean block (Machari Formation, South Korea). Our data from these successions capture two important global carbon-cycle perturbations, each of which are associated (in locations elsewhere) with significant faunal turnover in shallow-shelf communities—the SPICE and DICE events.

Our data, when combined with Fe-speciation data from the SGP database from five additional basins with stratigraphy spanning this time interval, reveal important trends for the broader role played by the redox structure of the ocean in the relationship between carbon-cycle perturbation and faunal turnover. Deeper-water (basin and outer-shelf) environments were predominantly anoxic and ferruginous throughout the studied interval and show little change associated with either of these events. The development of euxinic (free H_2S) conditions was uncommon both spatially and temporally. In instances where euxinia did develop, it was limited to areas where organic carbon and sulfate availability was high. Overall, beyond the first-order control of basinal position, local redox conditions were most highly influenced by sedimentation rates, with more highly-reducing conditions found to be generally associated with sites of lower sedimentation. These trends for deep water environments contrast with investigated shallower-water environments, which were primarily oxic during this time interval. However, these shallow environments do shift to more-reducing conditions during the SPICE.

The broad redox trends we document shed important light upon understanding the unusually high rates of faunal turnover (both rates of extinction and origination) seen across the later Cambrian. The repeated incursion and retreat of anoxic deep-waters onto the shallow shelf within a poorly-oxygenated deeper ocean would create environmental instability along shallow shelves. This instability produced the repeating pattern of extinction, replacement and diversification that has been observed during this time. While the trends in oceanic redox revealed by our study are consistent with the senario of the shoaling of poorly oxygenated waters causing these observed evolutionary patterns, the connection between marine redox and evolutionary records remains speculative. More data sets from this time interval, particularly from shallow environments, are needed that directly pair paleontological data with redox proxy data. Additionally, as noted earlier, the Fe speciation proxy is a fairly coarse proxy in regards to water column oxygenation as it can only potentially discern the presence and absence of oxygen. However, different animal groups have range of O_2 requirements and marine communities also have non-linear responses to changing O_2 levels (Sperling et al., 2015a). Thus, more refined reconstructions of changes in water column oxygenation, on biologically relevant scales, are also needed to more thoroughly evaluative the role that changing marine redox had on marine communities. Such future work on upper Cambrian and Lower Ordovician strata will help to clarify our understanding of a critical phase in the secular evolution of Earth's surficial environment, further illuminating the underlying causes and consequences of the late Cambrian "plateau" in biodiversity and how these changes set the stage for the rapid diversification of the GOBE.

Supplementary data to this article can be found online at https://doi.org/10.1016/j.palaeo.2020.110209.

Declaration of Competing Interest

The authors declare that they have no known competing financial interests or personal relationships that could have appeared to influence the work reported in this paper.

Acknowledgements

We'd thank editors Tom Algeo and Tim Lyons and Chadlin Ostrander and two other anonymous reviewers, all of whom provided comments that greatly improved our manuscript. Financial support for this work was provided by grants from the National Science Foundation Graduate Research Fellowship Program and the Virginia Tech Department of Geosciences awarded to MAL (2016). BCG would like to thank the Agouron Institute for post-doctoral support that helped fund the collection of the Machari Formation samples. EAS was funded by NSF EAR-1922966. NRM was funded by RGC-GRF-17303918. Russell Wheeler (VT '13) performed some of the lab work and analyses on samples from the Machari Formation (South Korea). We would like to thank Phil Wilby of the British Geological Survey for core access at the British Geological Survey, help sampling the Stockingford Shale Group samples, providing previously analyzed powders, and helpful discussion. Duck Choi is thanked for supporting the fieldwork on and collection of samples from the Machari Formation. This work resulted from activities of the Early Paleozoic Redox Working Group of the Sedimentary Geochemistry and Paleoenvironments Project (SGP), and we thank the SGP community and particularly Una Farrell for help sampling and with data management. Any opinions, findings, and conclusions or recommendations expressed in this material are those of the author(s) and do not necessarily reflect the views of the National Science Foundation.

References

Ahlberg, P., Axheimer, N., Babcock, L.E., Eriksson, M.E., Schmitz, B., Terfelt, F., 2009. Cambrian high-resolution biostratigraphy and carbon isotope chemostratigraphy in Scania, Sweden: first record of the SPICE and DICE excursions in Scandinavia. Lethaia 42, 2–16. https://doi.org/10.1111/j.1502-3931.2008.00127.x.

Aller, R.C., Mackin, J.E., Cox, R.T., 1986. Diagenesis of Fe and S in Amazon inner shelf muds: apparent dominance of Fe reduction and implications for the genesis of ironstones. Cont. Shelf Res. 6, 263–289. https://doi.org/10.1016/0278-4343(86)90064-6.

Aller, R.C., Madrid, V., Chistoserdov, A., Aller, J.Y., Heilbrun, C., 2010. Unsteady diagenetic processes and sulfur biogeochemistry in tropical deltaic muds: implications for oceanic isotope cycles and the sedimentary record. Geochim. Cosmochim. Acta 74, 4671–4692. https://doi.org/10.1016/j.gca.2010.05.008.

Anderson, T.F., Raiswell, R., 2004. Sources and mechanisms for the enrichment of highly reactive iron in euxinic Black Sea sediments. Am. J. Sci. 304, 203–233. https://doi.org/10.2475/ajs.304.3.203.

Babcock, L.E., Reichart, R.A., Rees, M.N., Peng, S., Saltzman, M.R., 2007. The Global boundary Stratotype Section and Point (GSSP) of the Drumian Stage (Cambrian) in the Drum Mountians, Utah, USA. Episodes 30, 85–95. https://doi.org/10.18814/epiiugs/2007/v30i2/003.

Babcock, L.E., Peng, S.-C., Brett, C.E., Zhu, M.-Y., Ahlberg, P., Bevis, M., Robison, R.A., 2015. Global climate, sea level cycles, and biotic events in the Cambrian Period. Palaeoworld 24, 5–15. https://doi.org/10.1016/j.palwor.2015.03.005.

Bambach, R.K., Knoll, A.H., Wang, S.C., 2004. Origination, extinction, and mass depletions of marine diversity. Paleobiology 30, 522–542. https://doi.org/10.1666/0094-8373(2004)030<0522:OEAMDO>2.0.CO;2.

Berner, R.A., 2006. GEOCARBSULF: a combined model for Phanerozoic atmospheric O_2 and CO_2. Geochim. Cosmochim. Acta 70, 5653–5664. https://doi.org/10.1016/j.gca.2005.11.032.

Brennan, S.T., Lowenstein, T.K., Horita, J., 2004. Seawater chemistry and the advent of biocalcification. Geology 32, 473–476. https://doi.org/10.1130/G20251.1.

Butterfield, N.J., 2009. Oxygen, animals and oceanic ventilation: an alternative view. Geobiology 7, 1–7. https://doi.org/10.1111/j.1472-4669.2009.00188.x.

Canfield, D.E., Raiswell, R., Westrich, J.T., Reaves, C.M., Berner, R.A., 1986. The use of chromium reduction in the analysis of reduced inorganic sulfur in sediments and shales. Chem. Geol. 54, 149–155. https://doi.org/10.1016/0009-2541(86)90078-1.

Canfield, D.E., Poulton, S.W., Narbonne, G.M., 2007. Late-Neoproterozoic deep-ocean oxygenation and the rise of animal life. Science 315, 92–95 (80). https://doi.org/10.1126/science.1135013.

Canfield, D.E., Poulton, S.W., Knoll, A.H., Narbonne, G.M., Ross, G., Goldberg, T., Strauss, H., 2008. Ferruginous conditions dominated later Neoproterozoic deep-water chemistry. Science 321, 949–952 (80). https://doi.org/10.1126/science.1154499.

Chen, X., Ling, H.-F., Vance, D., Shields-Zhou, G.A., Zhu, M., Poulton, S.W., Och, L.M., Jiang, S.-Y., Li, D., Cremonese, L., Archer, C., 2015. Rise to modern levels of ocean oxygenation coincided with the Cambrian radiation of animals. Nat. Commun. 6, 7142. https://doi.org/10.1038/ncomms8142.

Cheng, M., Li, C., Zhou, L., Algeo, T.J., Zhang, F., Romaniello, S., Jin, C.-S., Lei, L.-D., Feng, L.-J., Jiang, S.-Y., 2016. Marine Mo biogeochemistry in the context of dynamically euxinic mid-depth waters: a case study of the lower Cambrian Niutitang shales, South China. Geochim. Cosmochim. Acta 183, 79–93. https://doi.org/10.1016/j.gca.2016.03.035.

Cheng, M., Li, C., Zhou, L., Feng, L., Algeo, T.J., Zhang, F., Romaniello, S., Jin, C., Ling, H., Jiang, S., 2017. Transient deep-water oxygenation in the early Cambrian Nanhua Basin, South China. Geochim. Cosmochim. Acta 210, 42–58. https://doi.org/10.1016/j.gca.2017.04.032.

Choi, D.K., Lee, J.G., Lee, S.-B., Park, T.-Y.S., Hong, P.S., 2016. Trilobite biostratigraphy of the lower Paleozoic (Cambrian–Ordovician) Joseon Supergroup, Taebaeksan Basin, Korea. Acta Geol. Sin. - Eng. Ed. 90, 1976–1999. https://doi.org/10.1111/1755-6724.13016.

Chough, S.K., Kwon, S.-T., Ree, J.-H., Choi, D.K., 2000. Tectonic and sedimentary evolution of the Korean peninsula: a review and new view. Earth-Sci. Rev. 52, 175–235. https://doi.org/10.1016/S0012-8252(00)00029-5.

Clarkson, E.N.K., 2011. The life and times of the olenid trilobites. Geol. výzkumy na Moravě a ve Slezsku 18, 11–17.

Clarkson, E.K., Taylor, C.M., 1995. The lost world of the olenid trilobites. Geol. Today 11, 147–154. https://doi.org/10.1111/j.1365-2451.1995.tb00944.x.

Clarkson, M.O., Poulton, S.W., Guilbaud, R., Wood, R.A., 2014. Assessing the utility of Fe/Al and Fe-speciation to record water column redox conditions in carbonate-rich sediments. Chem. Geol. 382, 111–122. https://doi.org/10.1016/j.chemgeo.2014.05.031.

Cocks, Lr.M., Torsvik, T.H., 2016. Cambrian. In: Cocks, L.R.M., Torsvik, T.H. (Eds.), Earth History and Palaeogeography. Cambridge University Press, Cambridge, pp. 85–100. https://doi.org/10.1017/9781316225523.006.

Cole, D.B., Mills, D.B., Erwin, D.H., Sperling, E.A., Porter, S.M., Reinhard, C.T., Planavsky, N.J., 2020. On the co-evolution of surface oxygen levels and animals. Geobiology 1–22. https://doi.org/10.1111/gbi.12382.

Creveling, J.R., Johnston, D.T., Poulton, S.W., Kotrc, B., März, C., Schrag, D.P., Knoll, A.H., 2014. Phosphorus sources for phosphatic Cambrian carbonates. Bull. Geol. Soc. Am. 126, 145–163. https://doi.org/10.1130/B30819.1.

Cuggy, M.B., 1996. Patterns of faunal change at an upper Cambrian trilobite extinction event. In: Nolichucky Formation, Tennessee and Virginia. Masters Thesis Brock University (p. 142).

Dahl, T.W., Hammarlund, E.U., Anbar, A.D., Bond, D.P.G., Gill, B.C., Gordon, G.W., Knoll, A.H., Nielsen, A.T., Schovsbo, N.H., Canfield, D.E., 2010. Devonian rise in atmospheric oxygen correlated to the radiations of terrestrial plants and large predatory fish. Proc. Natl. Acad. Sci. 107, 17911–17915. https://doi.org/10.1073/pnas.1011287107.

Dahl, T.W., Boyle, R.A., Canfield, D.E., Connelly, J.N., Gill, B.C., Lenton, T.M., Bizzarro, M., 2014. Uranium isotopes distinguish two geochemically distinct stages during the later Cambrian SPICE event. Earth Planet. Sci. Lett. 401, 313–326. https://doi.org/10.1016/j.epsl.2014.05.043.

Dahl, T.W., Connelly, J.N., Li, D., Kouchinsky, A., Gill, B.C., Porter, S., Maloof, A.C., Bizzarro, M., 2019. Atmosphere–ocean oxygen and productivity dynamics during early animal radiations. Proc. Natl. Acad. Sci. 116, 19352–19361. https://doi.org/10.1073/pnas.1901178116.

Detmers, J., Bruchert, V., Habicht, K.S., Kuever, J., 2001. Diversity of sulfur isotope fractionations by sulfate-reducing prokaryotes. Appl. Environ. Microbiol. 67, 888–894. https://doi.org/10.1128/AEM.67.2.888-894.2001.

Edwards, C.T., Fike, D.A., Saltzman, M.R., Lu, W., Lu, Z., 2018. Evidence for local and global redox conditions at an early Ordovician (Tremadocian) mass extinction. Earth Planet. Sci. Lett. 481, 125–135. https://doi.org/10.1016/j.epsl.2017.10.002.

Elrick, M.B., Rieboldt, S.E., Saltzman, M.R., McKay, R.M., 2011. Oxygen-isotope trends and seawater temperature changes across the Late Cambrian Steptoean positive carbon-isotope excursion (SPICE event). Geology 39, 987–990. https://doi.org/10.1130/G32109.1.

Eriksson, M.E., Terfelt, F., 2007. Anomalous facies and ancient faeces in the latest middle Cambrian of Sweden. Lethaia 40, 69–84. https://doi.org/10.1111/j.1502-3931.2006.00007.x.

Faggetter, L.E., Wignall, P.B., Pruss, S.B., Sun, Y., Raine, R.J., Newton, R.J., Widdowson, M., Joachimski, M.M., Smith, P.M., 2018. Sequence stratigraphy, chemostratigraphy and facies analysis of Cambrian Series 2 - Series 3 boundary strata in northwestern Scotland. Geol. Mag. 155, 865–877. https://doi.org/10.1017/S0016756816000947.

Feng, L., Li, C., Huang, J., Chang, H., Chu, X., 2014. A sulfate control on marine mid-depth euxinia on the early Cambrian (ca. 529–521Ma) Yangtze platform, South China. Precambrian Res. 246, 123–133. https://doi.org/10.1016/j.precamres.2014.03.002.

Fortey, R.A., 1985. Pelagic trilobites as an example of deducing the life habits of extinct arthropods. Trans. R. Soc. Edinb. Earth Sci. 76, 219–230. https://doi.org/10.1017/S0263593300010452.

Fortey, R.A., 1989. There are extinctions and extinctions: examples from the lower Palaeozoic. Philos. Trans. R. Soc. Lond. Ser. B Biol. Sci. 325, 327–355. https://doi.org/10.1098/rstb.1989.0092.

Fortey, R.A., Wilmot, N.V., 1991. Trilobite cuticle thickness in relation to palaeoenvironment. Paläontol. Z. 65, 141–151. https://doi.org/10.1007/BF02985779.

Fortey, R., 2000. Olenid trilobites: the oldest known chemoautotrophic symbionts? Proc. Natl. Acad. Sci. 97, 6574–6578. https://doi.org/10.1073/pnas.97.12.6574.

Freeman, R.L., Miller, J.F., Dattilo, B.F., 2018. Linguliform brachiopods across a Cambrian-Ordovician (Furongian, early Ordovician) biomere boundary: the Sunwaptan-Skullrockian north American Stage boundary in the Wilberns and Tanyard formations of Central Texas. J. Paleontol. 92, 751–767. https://doi.org/10.1017/jpa.2018.8.

Fry, B., Gest, H., Hayes, J.M., 1984. Isotope effects associated with the anaerobic oxidation of sulfide by the purple photosynthetic bacterium, *Chromatium vinosum*. FEMS Microbiol. Lett. 22, 283–287. https://doi.org/10.1016/0378-1097(84)90025-9.

Fry, B., Cox, J., Gest, H., Hayes, J.M., 1986. Discrimination between 34S and 32S during bacterial metabolism of inorganic sulfur compounds. J. Bacteriol. 165, 328–330. https://doi.org/10.1128/jb.165.1.328-330.1986.

Fry, B., Ruf, W., Gest, H., Hayes, J.M., 1988. Sulfur isotope effects associated with oxidation of sulfide by O_2 in aqueous solution. Chem. Geol. 73, 205–210. https://doi.org/10.1016/0168-9622(88)90001-2.

Fry, B., Silva, S.R., Kendall, C., Anderson, R.K., 2002. Oxygen isotope corrections for online $\delta^{34}S$ analysis. Rapid Commun. Mass Spectrom. 16, 854–858. https://doi.org/10.1002/rcm.651.

Gerhardt, A.M., Gill, B.C., 2016. Elucidating the relationship between the later Cambrian end-Marjuman extinctions and SPICE Event. Palaeogeogr. Palaeoclimatol. Palaeoecol. 461, 362–373. https://doi.org/10.1016/j.palaeo.2016.08.031.

Gill, B.C., Lyons, T.W., Saltzman, M.R., 2007. Parallel, high-resolution carbon and sulfur isotope records of the evolving Paleozoic marine sulfur reservoir. Palaeogeogr. Palaeoclimatol. Palaeoecol. 256, 156–173. https://doi.org/10.1016/j.palaeo.2007.02.030.

Gill, B.C., Lyons, T.W., Young, S.A., Kump, L.R., Knoll, A.H., Saltzman, M.R., 2011. Geochemical evidence for widespread euxinia in the later Cambrian Ocean. Nature 469, 80–83. https://doi.org/10.1038/nature09700.

Glasspool, I.J., Scott, A.C., 2010. Phanerozoic concentrations of atmospheric oxygen reconstructed from sedimentary charcoal. Nat. Geosci. 3, 627–630. https://doi.org/10.1038/ngeo923.

Habicht, K.S., Canfield, D.E., 1997. Sulfur isotope fractionation during bacterial sulfate reduction in organic-rich sediments. Geochim. Cosmochim. Acta 61, 5351–5361. https://doi.org/10.1016/S0016-7037(97)00311-6.

Habicht, K.S., Canfield, D.E., 2001. Isotope fractionation by sulfate-reducing natural populations and the isotopic composition of sulfide in marine sediments. Geology 29, 555. https://doi.org/10.1130/0091-7613(2001)029<0555:IFBSRN>2.0.CO;2.

Hammarlund, E.U., Gaines, R.R., Prokopenko, M.G., Qi, C., Hou, X.-G., Canfield, D.E., 2017. Early Cambrian oxygen minimum zone-like conditions at Chengjiang. Earth Planet. Sci. Lett. 475, 160–168. https://doi.org/10.1016/j.epsl.2017.06.054.

Harper, D.A.T., Topper, T.P., Cascales-Miñana, B., Servais, T., Zhang, Y.-D., Ahlberg, P., 2019. The Furongian (late Cambrian) biodiversity gap: real or apparent? Palaeoworld 28, 4–12. https://doi.org/10.1016/j.palwor.2019.01.007.

Harries, P.J., Little, C.T.S., 1999. The early Toarcian (Early Jurassic) and the Cenomanian-Turonian (Late Cretaceous) mass extinctions: similarities and contrasts. Palaeogeography, Palaeoclimatology, Palaeoecology 154, 39–66. https://doi.org/10.1016/S0031-0182(99)00086–3.

He, T., Zhu, M., Mills, B.J.W., Wynn, P.M., Zhuravlev, A.Y., Tostevin, R., Pogge von Strandmann, P.A.E., Yang, A., Poulton, S.W., Shields, G.A., 2019. Possible links between extreme oxygen perturbations and the Cambrian radiation of animals. Nat. Geosci. 12, 468–474. https://doi.org/10.1038/s41561-019-0357-z.

Holland, H.D., 2002. Volcanic gases, black smokers, and the great oxidation event. Geochim. Cosmochim. Acta 66, 3811–3826. https://doi.org/10.1016/S0016-7037(02)00950-X.

Hong, P.S., 2014. Cambrian Series 3 Trilobites From the Lower Part of the Machari Formation, Deoksang Section, Yeongwol, Korea. Doctoral Disseration Seoul National University (p. 108).

Hong, P.S., Choi, D.K., 2015. Cambrian series 3 agnostoid trilobites *Ptychagnostus sinicus* and *Ptychagnostus atavus* from the Machari Formation, Yeongwol Group, Taebaeksan Basin, Korea. J. Paleontol. 89, 377–384. https://doi.org/10.1017/jpa.2015.30.

Hough, M.L., Shields, G.A., Evins, L.Z., Strauss, H., Henderson, R.A., Mackenzie, S., 2006. A major sulphur isotope event at c. 510 Ma: a possible anoxia-extinction-volcanism connection during the Early-Middle Cambrian transition? Terra Nova 18, 257–263. https://doi.org/10.1111/j.1365-3121.2006.00687.x.

Howley, R.A., Jiang, G., 2010. The Cambrian Drumian carbon isotope excursion (DICE) in the Great Basin, western United States. Palaeogeogr. Palaeoclimatol. Palaeoecol. 296, 138–150. https://doi.org/10.1016/j.palaeo.2010.07.001.

Hurtgen, M.T., Pruss, S.B., Knoll, A.H., 2009. Evaluating the relationship between the carbon and sulfur cycles in the later Cambrian Ocean: an example from the Port au Port Group, western Newfoundland, Canada. Earth Planet. Sci. Lett. 281, 288–297. https://doi.org/10.1016/j.epsl.2009.02.033.

Ingall, E., Jahnke, R., 1994. Evidence for enhanced phosphorus regeneration from marine sediments overlain by oxygen depleted waters. Geochim. Cosmochim. Acta 58, 2571–2575. https://doi.org/10.1016/0016-7037(94)90033-7.

Jin, C., Li, C., Algeo, T.J., Cheng, M., Lei, L., Zhang, Z., Shi, W., 2017. Evidence for marine redox control on spatial colonization of early animals during Cambrian age 3 (c. 521–514 Ma) in South China. Geol. Mag. 154, 1360–1370. https://doi.org/10.1017/S0016756816001138.

Jin, C., Li, C., Algeo, T.J., Planavsky, N.J., Cui, H., Yang, X., Zhao, Y., Zhang, X., Xie, S., 2016. A highly redox-heterogeneous ocean in South China during the early Cambrian (~529–514 Ma): implications for biota-environment co-evolution. Earth Planet. Sci. Lett. 441, 38–51. https://doi.org/10.1016/j.epsl.2016.02.019.

Johnston, D.T., Poulton, S.W., Dehler, C., Porter, S., Husson, J., Canfield, D.E., Knoll, A.H., 2010. An emerging picture of Neoproterozoic ocean chemistry: insights from the Chuar Group, Grand Canyon, USA. Earth Planet. Sci. Lett. 290, 64–73. https://doi.org/10.1016/j.epsl.2009.11.059.

Kaplan, I.R., Rittenberg, S.C., 1964. Microbiological fractionation of sulphur isotopes. J. Gen. Microbiol. 34, 195–212. https://doi.org/10.1099/00221287-34-2-195.

Kendall, B., Dahl, T.W., Anbar, A.D., 2017. The stable isotope geochemistry of molybdenum. Rev. Mineral. Geochem. 82, 683–732. https://doi.org/10.2138/rmg.2017.82.16.

Krause, A.J., Mills, B.J.W., Zhang, S., Planavsky, N.J., Lenton, T.M., Poulton, S.W., 2018. Stepwise oxygenation of the Paleozoic atmosphere. Nat. Commun. 9, 4081. https://doi.org/10.1038/s41467-018-06383-y.

Lehnert, O., Ahlberg, P., Calner, M., Joachimski, M.M., 2013. The Drumian Isotopic Carbon Excursion (DICE) in Scania, southern Sweden – A mirror of the onset of the Marjumiid Biomere at a time of increased primary production? In: Lindskog, A., Mehlqvist, K. (Eds.), 3rd IGCP 591 Annual Meeting. Lund University, Lund, Sweden, pp. 172–174.

Lenton, T.M., Boyle, R.A., Poulton, S.W., Shields-Zhou, G.A., Butterfield, N.J., 2014. Co-evolution of eukaryotes and ocean oxygenation in the Neoproterozoic era. Nat. Geosci. 7, 257–265. https://doi.org/10.1038/ngeo2108.

Lenton, T.M., Daines, S.J., Mills, B.J.W., 2018. COPSE reloaded: an improved model of biogeochemical cycling over Phanerozoic time. Earth-Sci. Rev. 178, 1–28. https://doi.org/10.1016/j.earscirev.2017.12.004.

LeRoy, Matthew A., Gill, B.C., 2019. Evidence for the development of local anoxia during the Cambrian SPICE event in eastern North America. Geobiology 17, 381–400. https://doi.org/10.1111/gbi.12334.

Li, D., Zhang, Xiaolin, Zhang, Xu, Zhu, H., Peng, S., Sun, L., Shen, Y., 2019. A paired carbonate–organic $\delta^{13}C$ approach to understanding the Cambrian Drumian carbon isotope excursion (DICE). Precambrian Res., 105503 https://doi.org/10.1016/j.precamres.2019.105503.

Li, C., Love, G.D., Lyons, T.W., Fike, D.A., Sessions, A.L., Chu, X., 2010. A stratified redox model for the Ediacaran ocean. Science 328, 80–83 (80). https://doi.org/10.1126/science.1182369.

Li, C., Jin, C., Planavsky, N.J., Algeo, T.J., Cheng, M., Yang, X., Zhao, Y., Xie, S., 2017. Coupled oceanic oxygenation and metazoan diversification during the early–middle Cambrian? Geology 39, 707–710. https://doi.org/10.1130/G39208.1.

Li, D., Zhang, Xiaolin, Hu, D., Chen, X., Huang, W., Zhang, Xu, Li, M., Qin, L., Peng, S., Shen, Y., 2018. Evidence of a large $\delta^{13}C_{carb}$ and $\delta^{13}C_{org}$ depth gradient for deep-water anoxia during the late Cambrian SPICE event. Geology 46, 631–634. https://doi.org/10.1130/G40231.1.

Loch, J.D., Stitt, J.H., Derby, J.R., 1993. Cambrian–Ordovician boundary interval extinctions: implications of revised trilobite and brachiopod data from Mount Wilson, Alberta, Canada. J. Paleontol. 67, 497–517. https://doi.org/10.1017/S0022336000024859.

Lu, W., Ridgwell, A., Thomas, E., Hardisty, D.S., Luo, G., Algeo, T.J., Saltzman, M.R., Gill, B.C., Shen, Y., Ling, H.-F., Edwards, C.T., Whalen, M.T., Zhou, X., Gutchess, K.M., Jin, L., Rickaby, R.E.M., Jenkyns, H.C., Lyons, T.W., Lenton, T.M., Kump, L.R., Lu, Z., 2018. Late inception of a resiliently oxygenated upper ocean. Science 361, 174–177. https://doi.org/10.1126/science.aar5372.

Ludvigsen, R., 1982. Upper Cambrian and Lower Ordovician Trilobite Biostratigraphy of the Rabbitkettle Formation, Western District of Mackenzie. Royal Ontario Museum, Toronto. https://doi.org/10.5962/bhl.title.52077.

März, C., Poulton, S.W., Beckmann, B., Küster, K., Wagner, T., Kasten, S., 2008. Redox sensitivity of P cycling during marine black shale formation: dynamics of sulfidic and anoxic, non-sulfidic bottom waters. Geochim. Cosmochim. Acta 72, 3703–3717. https://doi.org/10.1016/j.gca.2008.04.025.

McKenzie, N.R., Hughes, N.C., Gill, B.C., Myrow, P.M., 2014. Plate tectonic influences on Neoproterozoic–early Paleozoic climate and animal evolution. Geology 42, 127–130. https://doi.org/10.1130/G34962.1.

Mills, D.B., Canfield, D.E., 2014. Oxygen and animal evolution: did a rise of atmospheric oxygen "trigger" the origin of animals? BioEssays 36, 1145–1155. https://doi.org/10.1002/bies.201400101.

Mills, D.B., Ward, L.M., Jones, C., Sweeten, B., Forth, M., Treusch, A.H., Canfield, D.E., 2014. Oxygen requirements of the earliest animals. Proc. Natl. Acad. Sci. 111, 4168–4172. https://doi.org/10.1073/pnas.1400547111.

Ng, T.-W., Yuan, J.-L., Lin, J.-P., 2014. The North China Steptoean positive carbon isotope excursion and its global correlation with the base of the Paibian Stage (early Furongian Series), Cambrian. Lethaia 47, 153–164. https://doi.org/10.1111/let.12027.

Och, L.M., Shields-Zhou, G.A., 2012. The Neoproterozoic oxygenation event: environmental perturbations and biogeochemical cycling. Earth-Sci. Rev. 110, 26–57. https://doi.org/10.1016/j.earscirev.2011.09.004.

Och, L.M., Shields-Zhou, G.A., Poulton, S.W., Manning, C., Thirlwall, M.F., Li, D., Chen, X., Ling, H., Osborn, T., Cremonese, L., 2013. Redox changes in early Cambrian black shales at Xiaotan section, Yunnan Province, South China. Precambrian Res. 225, 166–189. https://doi.org/10.1016/j.precamres.2011.10.005.

Och, L.M., Cremonese, L., Shields-Zhou, G.A., Poulton, S.W., Struck, U., Ling, H., Li, D., Chen, X., Manning, C., Thirlwall, M., Strauss, H., Zhu, M., 2016. Palaeoceanographic controls on spatial redox distribution over the Yangtze Platform during the Ediacaran-Cambrian transition. Sedimentology 63, 378–410. https://doi.org/10.1111/sed.12220.

Owens, J.D., 2019. Application of thallium isotopes. In: Lyons, T.W., Turchyn, A.V., Reinhard, C.T. (Eds.), Elements in Geochemical Tracers in Earth System Science. Cambridge University Press, New York. https://doi.org/10.1017/9781108688697 (p. 21).

Pagès, A., Schmid, S., 2016. Euxinia linked to the Cambrian Drumian carbon isotope excursion (DICE) in Australia: geochemical and chemostratigraphic evidence. Palaeogeogr. Palaeoclimatol. Palaeoecol. 461, 65–76. https://doi.org/10.1016/j.palaeo.2016.08.008.

Pagès, A., Schmid, S., Edwards, D., Barnes, S., He, N., Grice, K., 2016. A molecular and isotopic study of palaeoenvironmental conditions through the middle Cambrian in the Georgina Basin, Central Australia. Earth Planet. Sci. Lett. 447, 21–32. https://doi.org/10.1016/J.EPSL.2016.04.032.

Palmer, A.R., 1965. Biomere: a new kind of biostratigraphic unit. J. Paleontol. 39, 149–153. Doi: papers3://publication/uuid/CB748D8B-6DFB-4EAA-8B74-0B5E4FC546A7.

Palmer, A.R., 1984. The Biomere problem: evolution of an idea. J. Paleontol. 58, 599–611.

Park, T., Choi, D.K., 2011. Trilobite faunal successions across the base of the Furongian Series in the Taebaek Group, Taebaeksan Basin, Korea. Geobios 44, 481–498. https://doi.org/10.1016/j.geobios.2011.02.003.

Pasquier, V., Sansjofre, P., Rabineau, M., Revillon, S., Houghton, J., Fike, D.A., 2017. Pyrite sulfur isotopes reveal glacial−interglacial environmental changes. Proc. Natl. Acad. Sci. 114, 5941–5945. https://doi.org/10.1073/pnas.1618245114.

Peng, S., Babcock, L.E., Robison, R.A., Lin, H., Rees, M.N., Saltzman, M.R., 2004. Global Standard Stratotype-section and Point (GSSP) of the Furongian series and Paibian Stage (Cambrian). Lethaia 37, 365–379. https://doi.org/10.1080/00241160410002081.

Peng, Y.Y., Peng, Y.Y., Lang, X., Ma, H., Huang, K., Li, F., Shen, B., 2016. Marine carbon-sulfur biogeochemical cycles during the Steptoean Positive Carbon Isotope Excursion (SPICE) in the Jiangnan Basin, South China. J. Earth Sci. 27, 242–254. https://doi.org/10.1007/s12583-016-0694-4.

Perfetta, P.J., Shelton, K.L., Stitt, J.H., 1999. Carbon isotope evidence for deep-water invasion at the Marjumiid-Pterocephaliid biomere boundary, Black Hills, USA: a common origin for biotic crises on late Cambrian shelves. Geology 27, 403–406. https://doi.org/10.1130/0091-7613(1999)027<0403:CIEFDW>2.3.CO;2.

Planavsky, N.J., Reinhard, C.T., Wang, X., Thomson, D., McGoldrick, P., Rainbird, R.H., Johnson, T., Fischer, W.W., Lyons, T.W., 2014. Low Mid-Proterozoic atmospheric oxygen levels and the delayed rise of animals. Science 346, 635–638 (80). https://doi.org/10.1126/science.1258410.

Poulton, S.W., Canfield, D.E., 2005. Development of a sequential extraction procedure for iron: implications for iron partitioning in continentally derived particulates. Chem. Geol. 214, 209–221. https://doi.org/10.1016/j.chemgeo.2004.09.003.

Poulton, S.W., Canfield, D.E., 2011. Ferruginous conditions: a dominant feature of the ocean through Earth's history. Elements 7, 107–112. https://doi.org/10.2113/gselements.7.2.107.

Poulton, S.W., Raiswell, R., 2002. The low-temperature geochemical cycle of iron: from continental fluxes to marine sediment deposition. Am. J. Sci. 302, 774–805. https://doi.org/10.2475/ajs.302.9.774.

Pruss, S.B., Finnegan, S., Fischer, W.W., Knoll, A.H., 2010. Carbonates in skeleton-poor seas: new insights from Cambrian and Ordovician Strata of Laurentia. Palaios 25, 73–84. https://doi.org/10.2110/palo.2009.p09-101r.

Pruss, S.B., Jones, D.S., Fike, D.A., Tosca, N.J., Wignall, P.B., 2019. Marine anoxia and sedimentary mercury enrichments during the late Cambrian SPICE event in northern Scotland. Geology 47, 1–4. https://doi.org/10.1130/G45871.1.

Pulsipher, M.A., Schiffbauer, J.D., Jeffrey, M.J., Huntley, J.W., Fike, D.A., Shelton, K.L., 2021. A meta-analysis of the Steptoean Positive Carbon Isotope Excursion: The SPICEraq database. Earth-Science Reviews 212, 103442. https://doi.org/10.1016/j.earscirev.2020.103442.

Raiswell, R., Canfield, D.E., 1998. Sources of iron for pyrite formation in marine sediments. Am. J. Sci. 298, 219–245. https://doi.org/10.2475/ajs.298.3.219.

Raiswell, R., Hardisty, D.S., Lyons, T.W., Canfield, D.E., Owens, J.D., Planavsky, N.J., Poulton, S.W., Reinhard, C.T., 2018. The iron paleoredox proxies: a guide to the pitfalls, problems and proper practice. Am. J. Sci. 318, 491–526. https://doi.org/10.2475/05.2018.03.

Rasmussen, C.M.Ø., Kröger, B., Nielsen, M.L., Colmenar, J., 2019. Cascading trend of early Paleozoic marine radiations paused by late Ordovician extinctions. Proc. Natl. Acad. Sci. U. S. A. 116, 7207–7213. https://doi.org/10.1073/pnas.1821123116.

Rieboldt, S.E., 2005. Inarticulate Brachiopods of the Late Maijumiid and Pterocephaliid Biomeres (Late Middle- Early Late Cambrian) of West-Central Utah and East-Central Nevada, U.S.A. Universoty of California, Berkeley. https://doi.org/10.1017/S0165115300023299.

Ries, J.B., Fike, D.A., Grotzinger, J.P., Pratt, L.M., Lyons, T.W., 2009. Superheavy pyrite ($\delta^{34}S_{pyr} > \delta^{34}S_{CAS}$) in the terminal Proterozoic Nama Group, southern Namibia: a consequence of low seawater sulfate at the dawn of animal life. Geology 37, 743–746. https://doi.org/10.1130/G25775A.1.

Rushton, A.W.A., 1978. Fossils from the Middle–Upper Cambrian transition in the Nuneaton district. Palaeontology 21, 245–283.

Rushton, A.W.A., 1983. Trilobites from the Upper Cambrian Olenus Zone in Central England. Spec. Pap. Palaeontol. 30, 107–139.

Saltzman, Matthew R., Runnegar, B., Lohmann, K.C., 1998. Carbon isotope stratigraphy of Upper Cambrian (Steptoean Stage) sequences of the eastern Great Basin: record of a global oceanographic event. Geol. Soc. Am. Bull. 110, 285–297. https://doi.org/10.1130/0016-7606(1998)110<0285:CISOUC>2.3.CO;2.

Saltzman, M.R., Ripperdan, R.L., Brasier, M.D., Lohmann, K.C., Reichart, R.A., Chang, W. T., Peng, S., Ergaliev, E.K., Runnegar, B., 2000. A global carbon isotope excursion (SPICE) during the Late Cambrian: relation to trilobite extinctions, organic-matter burial and sea level. Palaeogeogr. Palaeoclimatol. Palaeoecol. 162, 211–223. https://doi.org/10.1016/S0031-0182(00)00128-0.

Saltzman, M.R., Young, S.A., Kump, L.R., Gill, B.C., Lyons, T.W., Runnegar, B., 2011. Pulse of atmospheric oxygen during the late Cambrian. Proc. Natl. Acad. Sci. U. S. A. 108 https://doi.org/10.1073/pnas.1011836108.

Saltzman, M.R., Edwards, C.T., Adrain, J.M., Westrop, S.R., 2015. Persistent oceanic anoxia and elevated extinction rates separate the Cambrian and Ordovician radiations. Geology 43, 807–810. https://doi.org/10.1130/G36814.1.

Schachat, S.R., Labandeira, C.C., Saltzman, M.R., Cramer, B.D., Payne, J.L., Boyce, C.K., 2018. Phanerozoic pO2 and the early evolution of terrestrial animals. Proc. R. Soc. B Biol. Sci. 285 https://doi.org/10.1098/rspb.2017.2631.

Schiffbauer, J.D., Huntley, J.W., Fike, D.A., Jeffrey, M.J., Gregg, J.M., Shelton, K.L., 2017. Decoupling biogeochemical records, extinction, and environmental change during the Cambrian SPICE event. Science Advances 6. https://doi.org/10.1126/sciadv.1602158 e1602158.

Servais, T., Owen, A.W., Harper, D.A.T., Kröger, B., Munnecke, A., 2010. The Great Ordovician Biodiversification Event (GOBE): the palaeoecological dimension. Palaeogeogr. Palaeoclimatol. Palaeoecol. 294, 99–119. https://doi.org/10.1016/j.palaeo.2010.05.031.

Sheehan, P.M., 1996. A new look at Ecologic Evolutionary units (EEUs). Palaeogeogr. Palaeoclimatol. Palaeoecol. 127, 21–32. https://doi.org/10.1016/S0031-0182(96)00086-7.

Sim, M.S., Bosak, T., Ono, S., 2011a. Large Sulfur Isotope Fractionation does not require Disproportionation. Science 333, 74–77 (80). https://doi.org/10.1126/science.1205103.

Sim, M.S., Ono, S., Donovan, K., Templer, S.P., Bosak, T., 2011b. Effect of electron donors on the fractionation of sulfur isotopes by a marine Desulfovibrio sp. Geochim. Cosmochim. Acta 75, 4244–4259. https://doi.org/10.1016/j.gca.2011.05.021.

Slotznick, S.P., Sperling, E.A., Tosca, N.J., Miller, A.J., Clayton, K.E., van Helmond, N.A. G.M., Slomp, C.P., Swanson-Hysell, N.L., 2020. Unraveling the mineralogical complexity of sediment iron speciation using sequential extractions. Geochem. Geophys. Geosyst. 21 https://doi.org/10.1029/2019GC008666.

Smith, P.M., Brock, G.A., Paterson, J.R., 2020. Shelly fauna from the Cambrian (Miaolingian, Guzhangian) Shannon Formation and the SPICE event in the Amadeus Basin, Northern Territory. Alcheringa 44, 1–24. https://doi.org/10.1080/03115518.2019.1660405.

Sperling, E.A., Frieder, C.A., Raman, A.V., Girguis, P.R., Levin, L.A., Knoll, A.H., 2013. Oxygen, ecology, and the Cambrian radiation of animals. Proc. Natl. Acad. Sci. U. S. A. 110, 13446–13451. https://doi.org/10.1073/pnas.1312778110.

Sperling, Erik A., Knoll, A.H., Girguis, P.R., 2015a. The ecological physiology of Earth's second oxygen revolution. Annu. Rev. Ecol. Evol. Syst. 46, 215–235. https://doi.org/10.1146/annurev-ecolsys-110512-135808.

Sperling, Erik A., Wolock, C.J., Morgan, A.S., Gill, B.C., Kunzmann, M., Halverson, G.P., Macdonald, F.A., Knoll, A.H., Johnston, D.T., 2015b. Statistical analysis of iron geochemical data suggests limited late Proterozoic oxygenation. Nature 523, 451–454. https://doi.org/10.1038/nature14589.

Sperling, E.A., Balthasar, U., Skovsted, C.B., 2018. On the edge of exceptional preservation: insights into the role of redox state in Burgess Shale-type taphonomic windows from the Mural Formation, Alberta, Canada. Emerg. Top. Life Sci. 2, 311–323. https://doi.org/10.1042/etls20170163.

Stitt, J.H., 1975. Adaptive radiation, trilobite paleoecology, and extinction, Ptychaspidid Biomere, Late Cambrian of Oklahoma. Fossils Strata 4, 381–390.

Stookey, L.L., 1970. Ferrozine—a new spectrophotometric reagent for iron. Anal. Chem. 42, 779–781. https://doi.org/10.1021/ac60289a016.

Strauss, J.V., Fraser, T., Melchin, M.J., Allen, T.J., Malinowski, J., Feng, X., Taylor, J.F., Day, J., Gill, B.C., Sperling, E.A., 2020. The Road River Group of northern Yukon, Canada: early Paleozoic deep-water sedimentation within the Great American Carbonate Bank. Can. J. Earth Sci. 27, 1–27. https://doi.org/10.1139/cjes-2020-0017.

Sundberg, F.A., 1991. Paleogeography of western Utah and eastern Nevada during the Ehmaniella biochron (Middle Cambrian). In: Cooper, J.D., Stevens, C.H. (Eds.), Paleozoic Paleogeography of the Western United States. SEPM (Society for Sedimentary Geology), pp. 387–399.

Sundberg, F.A., 1994. Corynexochida and Ptychopariida (Trilobita, Arthropoda) of the Ehmaniella Biozone (Middle Cambrian), Utah and Nevada, 446. Museum Nat. Hist. Contrib. Sci., Los Angeles, p. 137.

Taylor, J.F., 2006. History and status of the biomere concept. Mem. Assoc. Australas. Palaeontol. 32, 247–265.

Taylor, K., Rushton, A.W.A., 1971. The pre-Westphalian geology of the Warwickshire Coalfield. Bull. Geol. Surv. Gt. Britain 35.

Taylor, J.F., Repetski, J.E., Loch, J.D., Leslie, S.A., 2012. Biostratigraphy and chronostratigraphy of the Cambrian–Ordovician Great American Carbonate Bank. In: Derby, J.R., Fritz, R.D., Longacre, S.A., Morgan, W.A., Sternbach, C.A. (Eds.), The Great American Carbonate Bank: The Geology and Economic Resources of the Cambrian-Ordovician Sauk Megasequence of Laurentia, 98. AAPG Memoir, pp. 15–35. https://doi.org/10.1306/13331488M983497.

Viollier, E., Inglett, P.W., Hunter, K., Roychoudhury, A.N., Van Cappellen, P., 2000. The ferrozine method revisited: Fe(II)/Fe(III) determination in natural waters. Appl. Geochem. 15, 785–790. https://doi.org/10.1016/S0883-2927(99)00097-9.

Wang, J., Chen, D., Yan, D., Wei, H., Xiang, L., 2012. Evolution from an anoxic to oxic deep ocean during the Ediacaran–Cambrian transition and implications for bioradiation. Chem. Geol. 306–307, 129–138. https://doi.org/10.1016/j.chemgeo.2012.03.005.

Westrop, S.R., Ludvigsen, R., 1987. Biogeographic control of trilobite mass extinction at an Upper Cambrian "biomere" boundary. Paleobiology 13, 84–99. https://doi.org/10.1017/S0094837300008605.

Williams, M., Vannier, J., Corbari, L., Massabuau, J.-C., 2011. Oxygen as a driver of early arthropod micro-benthos evolution. PLoS One 6, e28183. https://doi.org/10.1371/journal.pone.0028183.

Wood, R., Erwin, D.H., 2018. Innovation not recovery: dynamic redox promotes metazoan radiations. Biol. Rev. 93, 863–873. https://doi.org/10.1111/brv.12375.

Woods, M.A., Wilby, P.R., Leng, M.J., Rushton, A.W.A., Williams, M., 2011. The Furongian (late Cambrian) Steptoean Positive Carbon Isotope Excursion (SPICE) in

Avalonia. J. Geol. Soc. Lond. 168, 851–862. https://doi.org/10.1144/0016-76492010-111.

Wotte, T., Strauss, H., 2015. Questioning a widespread euxinia for the Furongian (Late Cambrian) SPICE event: indications from δ13C, δ18O, δ34S and biostratigraphic constraints. Geol. Mag. 152, 1085–1103. https://doi.org/10.1017/S0016756815000187.

Zhu, M.-Y., Zhang, J.-M., Li, G.-X., Yang, A.-H., 2004. Evolution of C isotopes in the Cambrian of China: implications for Cambrian subdivision and trilobite mass extinctions. Geobios 37, 287–301. https://doi.org/10.1016/j.geobios.2003.06.001.